European Journal of Medicinal Chemistry 214 (2021) 113225

Contents lists available at ScienceDirect

European Journal of Medicinal Chemistry

journal homepage: http://www.elsevier.com/locate/ejmech

Synthesis, biological evaluation and structure-activity relationship of novel dichloroacetophenones targeting pyruvate dehydrogenase kinases with potent anticancer activity

Biao Xu [a, 1], Zhi-Peng Wang [b, d, 1], Qingwang Liu [e, 1], Xiaohong Yang [a], Xuemin Li [a], Ding Huang [a], Yanfei Qiu [a], Kin Yip Tam [c], Shao-Lin Zhang [a, **], Yun He [a, *]

[a] School of Pharmaceutical Sciences, Chongqing Key Laboratory of Natural Product Synthesis and Drug Research, Chongqing University, Chongqing, 401331, PR China
[b] Chongqing Institute of Green and Intelligent Technology, Chinese Academy of Sciences, Chongqing, PR China
[c] Faculty of Health Sciences, University of Macau, Taipa, Macau, PR China
[d] Chongqing School, University of Chinese Academy of Sciences Chongqing, PR China
[e] Institute of Health and Medical Technology, Hefei Institutes of Physical Science, Chinese Academy of Sciences, Hefei, Anhui, 230031, PR China

ARTICLE INFO

Article history:
Received 4 September 2020
Received in revised form
16 January 2021
Accepted 21 January 2021
Available online 28 January 2021

Keywords:
Pyruvate dehydrogenase kinase
Proliferation
Cancer metabolism
Structure-activity relationship

ABSTRACT

Pyruvate dehydrogenase kinases (PDKs) are promising therapeutic targets that have received increasing attentions in cancer metabolism. In this paper, we report the synthesis and biological evaluation of a series of novel dichloroacetophenones as potent PDKs inhibitors. Structure-activity relationship analysis enabled us to identify a potent compound **6u**, which inhibited PDKs with an EC_{50} value of 0.09 μM, and reduced various cancer cells proliferation with IC_{50} values ranging from 1.1 to 3.8 μM, while show weak effect against non-cancerous L02 cell (IC_{50} > 10 μM). In the A375 xenograft model, **6u** displayed an obvious antitumor activity at a dose of 5 mg/kg, but with no negative effect to the mice weight. Molecular docking suggested that **6u** formed direct hydrogen bond interactions with Ser75 and Gln61 in PDK1, and meanwhile the aniline skeleton in **6u** was sandwiched by the conserved hydrophobic residues Phe78 and Phe65, which contribute to the biochemical activity improvement. Moreover, **6u** induced A375 cell apoptosis and cell arrest in G1 phase, and inhibited cancer cell migration. In addition, **6u** altered glucose metabolic pathway in A375 cell by decreasing lactate formation and increasing ROS production and OCR consumption, which could serve as a potential modulator to reprogram the glycolysis pathway in cancer cell.

1. Introduction

Proliferating cancer cells exhibit a metabolic alteration, featuring increased glycolysis and suppressed oxidative phosphorylation in mitochondria, even under aerobic conditions [1,2]. These altered metabolic pathways are known to derive from oncogene mutations and aberrant protein expressions [3]. Targeting these mutated oncogenes and overexpressed proteins in metabolic pathways is thus considered promising therapeutic opportunities in cancer treatment [4,5].

One well-researched connection between glycolysis and oxidative phosphorylation pathway is pyruvate dehydrogenase complex (PDC) [6], which directly converts pyruvate into acetyl-CoA by the action of pyruvate dehydrogenase and is the gatekeeping enzyme linking the glycolysis and the oxidative phosphorylation [7]. PDC activity is mediated primarily by reversible phosphorylation, in which phosphorylation of any one of three serine residues on the alpha subunit of pyruvate dehydrogenase renders the enzyme inactive [8,9]. Phosphorylation of PDC is catalyzed by four isoforms of PDKs in human, namely PDK1-4, which has been widely observed in various human solid tumors [10] and linked to the oncogenic activation of AKT and HIF pathways that are integrated in the aberrant cancer metabolism [11]. Moreover, the continually overexpressed PDKs protein can be hijacked by cancer cells to inactivate PDC, which contributes to the

** Corresponding author.
* Corresponding author.
E-mail addresses: zhangsl@cqu.edu.cn (S.-L. Zhang), yun.he@cqu.edu.cn (Y. He).
[1] B. Xu, Z.-P. Wang and Q. W. Liu contributed equally to this study.

https://doi.org/10.1016/j.ejmech.2021.113225
0223-5234/

Warburg-identified glycolytic alterations [7]. Furthermore, it has been shown that the knockdown of PDKs restores PDC to a normal level and reverses these glycolytic effects [12]. Therefore, down-regulating PDKs activity by inhibitors would be an ideal strategy to modulate the dysregulated pyruvate metabolic pathway, thus providing a promising approach for killing or, at least, greatly reducing the growth of cancer cells.

So far, a number of compounds have been disclosed to inhibit PDKs activity [13–19], but none of them has successfully advanced into clinical application. **AZD7545** is a PDKs inhibitor with a trifluoromethylpropanamide warhead projecting to the lipoamide-binding site of PDKs and forms a direct hydrogen bond interaction with Ser75, while the 2-chlorophenyl group of **AZD7545** is sandwiched by the conserved hydrophobic residues Phe78 and Phe65, as shown in Fig. 1B. Another well-known PDKs inhibitor is dichloroacetate (**DCA**), which was used to treat patients with mitochondrial abnormalities [20], and has recently been studied in a clinical trial for cancer treatment [21]. However, its high efficacious dosage hampered its further clinical applications [22]. Dichloroacetophenone (**DAP**) is a **DCA** derivative that was discovered from a high-throughput screening campaign by GSK [23]. In addition, **DAP** weakly reduced A549 cancer cell proliferation, with an IC_{50} value of 15.9 μM. Moreover, the compound displayed only a 36.6% inhibitory rate at the tested concentration of 80 μM in a biochemical assay, which was clearly far from our satisfactory [24]. We previously reported the chemical modification of **DAP**, leading to the discovery of **DAP-64** (Fig. 1A), which inhibited PDKs activity (EC_{50} = 0.33 μM) and cancer cells proliferation (IC_{50} = 3.87 μM against A549) [25]. Continuing our efforts in discovering novel cancer metabolic modulators [19,26], herein we report the synthesis, biological evaluation, and structure-activity relationship analysis of a series of novel dichloroacetophenones targeting PDKs, which displayed an improved enzymatic potency and cellular activity as compared to **DAP** and **DAP-64**.

2. Results and discussion

2.1. Chemistry and design of the target compounds

The general synthetic routes for the designed dichloroacetophenones **3a-f** and **6a-u** were shown in Schemes 1-3. As shown in Scheme 1, 4-bromo-3-nitroacetophenone (**1**) reacted with various boronic acids in water/dioxane (v/v, 1:3) to afford **2a-f** by coupling reaction catalyzed by $Pd(PPh_3)_4$ or $Pd(OAc)_2$, which were then chlorinated in DMF with copper(II) chloride dehydrate and lithium chloride at 90 °C for 9 h to give the target compounds **3a**-**f**. However, we failed to obtain compounds **6a-s** using the same synthetic routes. Instead, we first prepared the dichloroacetophenone (**5**) by chlorinating **4** in acetonitrile with 2 equivalents of 1,3-dichloro-5,5-dimethylhydantoin (DCDMH) at 35 °C for 18 h. The fluorine group in **5** was then substituted by various primary amines or secondary amines to furnish a series of novel dichloroacetophenones (**6a**-**s**), as shown in Scheme 2.

In our molecular simulation assay, we found that the R^2 groups in **6a-s** projected into the lipoyl-binding pocket in PDK, where adjacent to the Ser75 residue. We expected that if we introduced a hydrogen bond donor into the end of R^2 group to form a direct hydrogen bond interaction with Ser75 in PDK, which would contribute to biochemical activity improvement. Bearing this in mind, we therefore designed **6t** and **6u**. As shown in Schemes 3 and 1-(4-aminophenyl)ethan-1-one (**7**) reacted with a methyl Grignard reagent at −10 °C for 3 h to form 2-(4-aminophenyl)propan-2-ol (**8**), which coupled with the dichloroacetophenone (**5**) to afford the target compound **6t**. Meanwhile, 2-(4-nitrophenyl)acetic acid (**9**) was esterified by CH_3OH to give methyl 2-(4-nitrophenyl)acetate (**10**), and reacted with iodomethane in DMF to form compound **11**, which was then reduced by DIBAL-H to generate 2-methyl-2-(4-nitrophenyl)propan-1-ol (**12**). Finally, **12** was reduced and coupled with dichloroacetophenone (**5**) to afford the target compound **6u**. All the dichloroketones were characterized by NMR and HRMS spectra, and their purities were confirmed by HPLC with no less than 95% (see Supporting Information).

2.2. Structure-activity relationship analysis

The dichloroacetophenones **3a-f** and **6a-u** were evaluated for their antiproliferative activity on MCF-7 and A549 cell lines at 1 and 10 μM, respectively, and the PDKs enzymatic activity was measured at 1 μM. The results of these biological evaluations are summarized in Table 1. **DAP** displayed poor antiproliferative activities against the two cancer cell lines at both tested concentrations, and barely inhibited PDKs activity at 1 μM. **DAP-64** exhibited improved cellular and biochemical activities as compared with **DAP**, which is in perfect agreement with our previous results [24,25].

The introduction of various aromatic substituents at 4-position of 2,2-dichloro-1-(3-nitrophenyl)ethan-1-one yielded a series of dichloroacetophenones (**3a-f**), which exhibited significant improvement of anticancer inhibitory activities as compared with **DAP** (Table 1). However, the PDKs inhibitions by these compounds were weak, with EC_{50} values were more than 10 μM, suggesting that other mechanisms, not just PDKs inhibition could be involved in their anti-proliferative effects. While keeping the nitro and

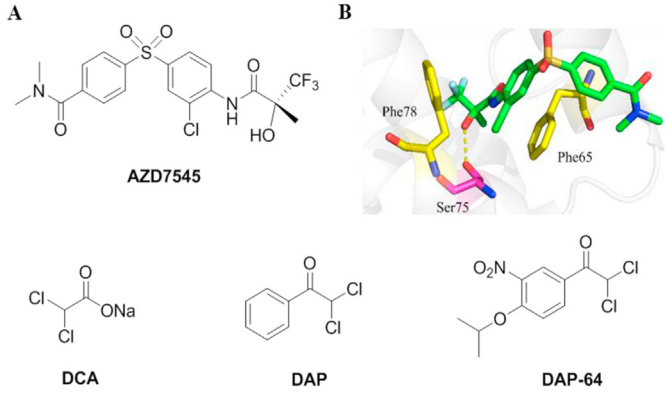

Fig. 1. (A) Chemical structures of the reported PDKs inhibitors. (B) Binding model of **AZD7545** with PDK1 (PDB code: 2Q8G).

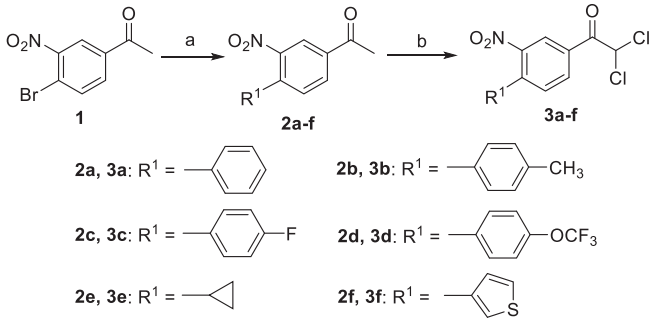

Scheme 1. Synthetic of dichloroacetophenones **3a-f**. Reaction conditions and reagents: (a) For **2a-d** and **2f**, boronic acids, K_2CO_3, $Pd(PPh_3)_4$, water/dioxane (v/v, 1:3), 95 °C, 6 h. For **2e**, cyclopropylboronic acid, tricyclohexyl phosphine, K_3PO_4, $Pd(OAc)_2$, water/dioxane (v/v, 1:3), 100 °C, 4 h. (b) Copper(II) chloride dehydrate, lithium chloride, DMF, 90 °C, 9 h.

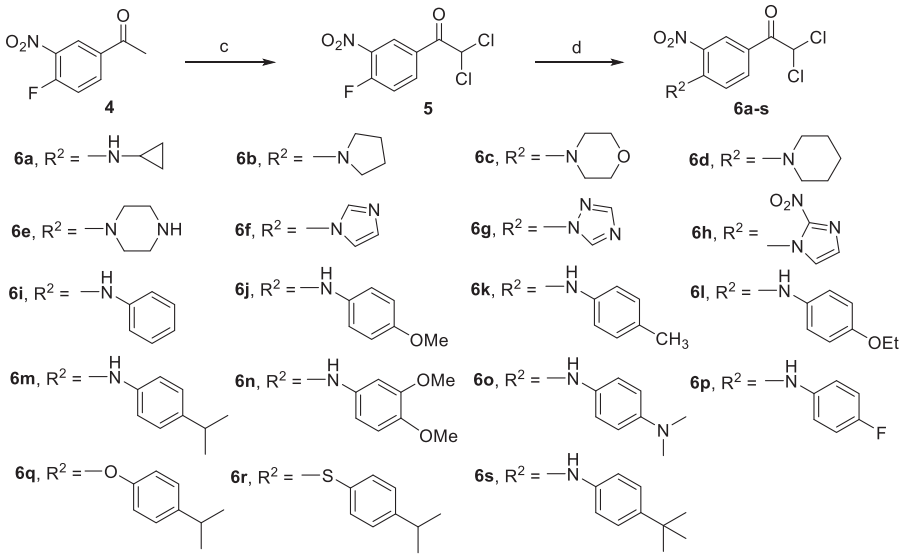

Scheme 2. Synthetic of dichloroacetophenones **6a-s**. Reaction conditions and reagents: (c) NH_4Cl, acetonitrile, DCDMH, 18 h, 35 °C. (d) Various primary amines or secondary amines, K_2CO_3, DMF, rt, 3 h.

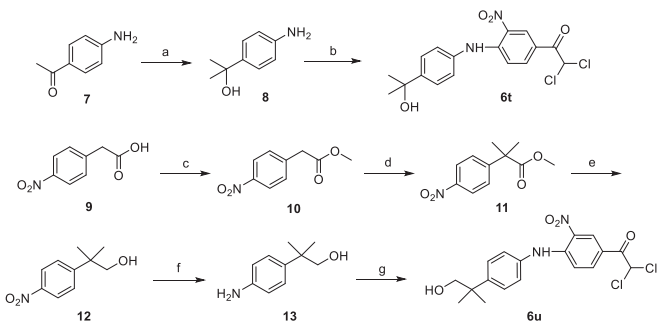

Scheme 3. Synthesis of compounds **6t** and **6u**. Reaction conditions and reagents: (a) CH_3MgBr, THF, −10 °C, 3 h. (b) K_2CO_3, dichloroacetophenone **5**, DMF, 12 h. (c) H_2SO_4, CH_3OH, reflux. (d) CH_3I, NaOH, DMF, 0 °C, 24 h. (e) DIBAL-H, THF, 0 °C. (f) Pd/C, H_2, EtOH, rt, 12 h. (g) K_2CO_3, dichloroacetophenone **5**, DMF, 12 h.

dichloroacetophenone groups unchanged, the replacement of the fluorine atom in compound **5** by cyclopropylamino, pyrrolidinyl, morpholinyl, piperidinyl, and piperazinyl groups afford a series of dichloroacetophenones (**6a**-**6e**), but they displayed a negligible improvement of PDKs inhibition at 1 μM as compared to **3a**-**f**. The potencies were greatly improved when some aniline substituents were incorporated at the same position. Especially, **6m** and **6s** exhibited dramatic improvements in biochemical activities, with the PDK inhibitory rates are 80.0 and 65.8% at 1 μM. Then we measured a full-dose response inhibition of the compounds on PDK, as shown in Table 2, the EC_{50} values are 0.34 and 0.55 μM for **6m** and **6s**, respectively. According our previous study [24], **DAP-64** bound to the hydrophobic lipoamide-binding site in PDK. We then docked **6m** and **6s** into the pocket, indicating that the substituted anilines were sandwiched by the conserved hydrophobic residues Phe78 and Phe65 in PDK (Fig. 2), which attributed to the biochemical activity improvement. The replacement of the −NH in **6m** by an oxygen (**6q**) or sulfur atom (**6r**) led to decrease of enzymatic activity, which might be explained by the restricted hydrophobic interaction between the benzene ring and Phe78 and Phe65 residues.

Compound **6m** gave an EC_{50} value of 0.34 μM against PDK, and inhibited the growth of cancer cell lines with IC_{50} values ranging from 0.33 to 1.2 μM, which suggest that **6m** is not a specific PDK inhibitor. We then modified **6m** by incorporating a hydroxyl group into the end of isopropylaniline skeleton to form **6t**, though a direct hydrogen bond interaction generated between **6t** and Ser75 (Fig. 3), the Phe78 is far away from the isopropylaniline skeleton, the sandwiched hydrophobic interaction disappeared, so the PDK inhibitory potency was slightly improved. While introducing a hydroxymethyl group into **6m** to afford compound **6u**, which not only retain the sandwich hydrophobic interaction, but also picked up hydrogen bond interactions with Ser75 and Gln61. As expected, **6u** displayed an improved PDK inhibitory potency, with an EC_{50} value of 0.09 μM, which outperform **6m** and **DAP-64.** We finally measured anticancer activity of **6m**, **6s**, **6t** and **6u** on various human derived solid cancer cells, all four compounds exhibited promising anticancer activities, with IC_{50} values ranging from 0.31 to 8.1 μM. Meanwhile, **6m-t** showed some cytotoxicity to L02 cell (IC_{50} = 1.5−7.8 μM), but not for **6u** and **DAP-64** in a high concentration.

2.3. Compound *6u* bound to PDK isoforms

PDKs protein contains four sub-type isoforms, namely PDK1-4. So next we have interest to explore the selective profile of **6u**. Firstly, we aligned the amino acids sequence of the lipoamide-binding site of PDK1-4, as shown in Fig. 4A. The Ser75, Phe78, and Phe65 residues in PDK1 is conserved in PDK2-4, suggesting **6u** might be a pan-isoform PDK inhibitor. We then docked **6u** to PDK2-4. However, the binding model for PDK2-4 is totally different from PDK1. The **6u** reaches into the deep lipoamide-binding pocket in PDK2, missing the hydrogen bond interaction with Ser49 (Fig. 4B), while for PDK4, **6u** retains the Ser53 hydrogen bond interaction, but missing the sandwiched hydrophobic interaction with Phe56 and Phe43 (Fig. 4D). In PDK3, **6u** picked up an additional interaction with a residue Lys173, which is a crucial amino acid in L2 domain in PDC (Fig. 4C). Finally, we titrated **6u** into PDK1-4 solution, and measured K_d values using an isothermal titration calorimetry (ITC) analysis. As shown in Fig. 4E and Fig S1 (see Supporting Information), the binding affinity for **6u** to PDK1 is 0.21 μM, much higher than PDK2-4. According to our molecular docking study, **6u**

Table 1
Biological evaluation of the prepared compounds **3a-f** and **6a-u**.

Comps	Antiproliferative inhibitory rate (%)				PDKs inhibition (%) at 1 μM [a]
	MCF-7		A549		
	10 (μM)	1 (μM)	10 (μM)	1 (μM)	
3a	56.2 ± 1.4	15.8 ± 1.1	92.6 ± 0.6	8.9 ± 1.4	25.6 ± 0.5
3b	89.1 ± 1.8	26.4 ± 2.3	96.0 ± 1.8	13.8 ± 2.8	5.9 ± 1.1
3c	91.6 ± 1.1	30.8 ± 3.5	95.3 ± 1.0	44.7 ± 4.0	12.1 ± 0.8
3d	97.8 ± 0.88	24.7 ± 3.7	93.6 ± 0.95	36.3 ± 3.1	21.4 ± 3.8
3e	87.8 ± 3.3	31.3 ± 6.5	95.9 ± 2.1	40.1 ± 4.2	17.3 ± 2.2
3f	43.5 ± 2.9	7.5 ± 3.7	94.4 ± 2.1	14.4 ± 2.8	26.5 ± 4.1
6a	96.0 ± 0.2	25.7 ± 2.1	95.7 ± 0.54	21.6 ± 1.9	17.5 ± 5.2
6b	94.6 ± 2.4	23.0 ± 4.2	97.3 ± 0.34	30.6 ± 0.11	32.4 ± 2.7
6c	90.4 ± 1.2	18.9 ± 3.9	95.6 ± 1.6	10.1 ± 3.2	36.9 ± 3.9
6d	95.8 ± 0.35	22.4 ± 4.9	97.1 ± 1.7	38.9 ± 1.7	40.2 ± 10.1
6e	57.0 ± 2.3	NH	93.1 ± 2.2	22.6 ± 2.4	48.6 ± 2.5
6f	90.5 ± 2.5	24.2 ± 5.3	96.6 ± 0.30	30.5 ± 3.5	20.5 ± 3.3
6g	11.9 ± 4.0	NI[b]	58.9 ± 1.6	NI	17.4 ± 2.8
6h	21.4 ± 0.9	NI	80.9 ± 0.81	NI	8.1 ± 1.2
6i	97.1 ± 0.52	26.3 ± 1.2	97.4 ± 1.2	46.1 ± 7.2	60.7 ± 7.3
6j	95.9 ± 0.18	29.2 ± 3.5	97.7 ± 0.36	45.0 ± 4.4	55.7 ± 4.1
6k	88.9 ± 1.8	12.1 ± 2.2	97.3 ± 1.1	48.1 ± 4.3	64.4 ± 4.7
6l	93.8 ± 2.0	18.8 ± 5.1	97.4 ± 0.70	52.9 ± 3.7	68.7 ± 3.6
6m	94.0 ± 0.8	38.6 ± 3.3	97.0 ± 1.7	75.2 ± 6.5	80.0 ± 7.9
6n	90.5 ± 2.5	24.2 ± 5.3	96.6 ± 0.30	40.5 ± 3.5	66.4 ± 7.5
6o	93.2 ± 1.3	31.6 ± 2.5	98.6 ± 0.8	75.0 ± 4.4	88.2 ± 5.8
6p	97.8 ± 1.6	17.9 ± 4.2	98.9 ± 0.2	23.2 ± 1.4	50.1 ± 2.3
6q	85.7 ± 5.8	28.7 ± 4.0	90.7 ± 3.4	12.5 ± 1.0	39.4 ± 1.7
6r	79.8 ± 7.1	18.9 ± 3.2	76.3 ± 2.5	12.9 ± 2.7	19.5 ± 5.8
6s	96.4 ± 7.1	41.2 ± 4.7	93.2 ± 3.8	48.8 ± 5.8	65.8 ± 9.7
6t	92.8 ± 3.2	33.9 ± 7.8	96.3 ± 5.8	37.9 ± 2.2	48.8 ± 3.3
6u	95.3 ± 4.8	38.9 ± 8.8	98.6 ± 7.5	29.4 ± 7.6	98.7 ± 10.4
DAP	42.2 ± 5.3	NI	55.2 ± 4.8	NI	36.6 ± 4.4 [c]
DAP-64	73.4 ± 3.7	NI	98.2 ± 7.8	18.7 ± 1.7	72.4 ± 10.0
AZD7545	NI	NI	NI	NI	98.7 ± 3.3
DOX[d]	97.5 ± 0.21	59.8 ± 1.2	98.5 ± 0.81	81.2 ± 0.6	NT[e]

[a] The PDKs inhibition rates were measured by the primary PDC enzymatic activity assay in the presence of the prepared compounds at 1 μM. The initial screen of cancer cells proliferative inhibition rates (%) was run by using the MTT assay. Both bioassays were three independent measurements, and the values were reported as the average ± S.D; [b] NI represents no inhibition; [c] PDKs inhibition rate was 36.6% for DAP at 80 μM; [d] DOX represents Doxorubicin, a clinical anticancer drug, which was used a positive control in the MTT assay; [e] NT represents not tested.

Table 2
Effects of some selected compounds (**6m**, **6s**, **6t**, and **6u**) on the growth of various cancer cell line human normal cell L02 (IC_{50}, μM) and PDKs function (EC_{50}, μM).

Comps.	IC_{50} (μM)							PDKs (EC_{50}, μM)
	A549	MCF-7	SHSY-5Y	HCT116	A375	PC-3	L02	
6m	0.33 ± 0.09	1.21 ± 0.30	1.0 ± 0.21	0.7 ± 0.11	0.9 ± 0.12	0.38 ± 0.05	1.5 ± 0.12	0.34 ± 0.07
6s	1.2 ± 0.17	1.9 ± 0.22	1.1 ± 0.15	0.5 ± 0.08	0.9 ± 0.11	0.47 ± 0.07	5.9 ± 0.84	0.55 ± 0.11
6t	3.1 ± 0.50	2.98 ± 0.55	2.3 ± 0.41	1.5 ± 0.22	1.8 ± 0.17	2.34 ± 0.30	7.8 ± 0.34	1.49 ± 0.20
6u	3.2 ± 0.14	2.4 ± 0.15	1.7 ± 0.23	2.1 ± 0.31	1.1 ± 0.14	3.8 ± 0.45	14.4 ± 0.85	0.09 ± 0.01
DAP-64	3.5 ± 0.11	7.8 ± 1.4	5.6 ± 0.9	6.2 ± 1.1	4.9 ± 0.8	8.7 ± 1.3	16.9 ± 1.1	0.33 ± 0.07
DAP	18.7 ± 1.6	21.4 ± 4.0	17.7 ± 1.5	12.9 ± 1.7	16.9 ± 2.5	23.1 ± 2.0	19.7 ± 1.1	>80
AZD7545	NI [a]	NI	NI	NI	NI	NI	NI	0.053
DCA [b]	19.5 ± 2.1	13.4 ± 0.9	17.4 ± 2.5	9.8 ± 0.15	20.1 ± 3.3	15.7 ± 1.4	21.7 ± 3.1	>100

[a] NI indicates no inhibitory activity.
[b] the unit of IC_{50} values of cell viability for DCA is mM.

exhibited the highest total binding scores with PDK3, but showed a relative weak binding affinity to PDK3 in the ITC titration process, which could be explained by the absence of the L2 domain in protein solution in the titration process.

2.4. Compound *6u* induced A375 cell apoptosis and cell cycle arrest in G1 phase

Since **6u** exhibited the most potent enzymatic potency, it was selected for further biological test. First, A375 cell was treated with **6u** (1, 2.5, and 5 μM) or **DAP-64** (5 μM) for 36 h, then stained with FITC Annexin V/PI dyes. As shown in Fig. 5, the percentages of apoptotic population in A375 cell treated with **6u** were 14.07, 27.90 and 51.27%, respectively, suggesting the induction of the apoptosis in A375 cells by **6u** followed a dose-dependent manner, while for **DAP-64** at 5 μM, the percentages was 28.82%. Furthermore, we measured the percentages of apoptotic population by **6u** for 12, and 24 h, respectively, and as shown in Fig. 6, the apoptosis rates were 15.58% at 12 h, and 25.58% for 24 h, following a time-dependent manner.

We then examined the effect of **6u** on cell cycle distribution using the propidium iodide (PI) staining kit. A375 cells were treated with **6u** (1, 2.5, and 5 μM) or **DAP-64** (5 μM) for 24 h, then stained with PI and analyzed on a flow cytometer. As shown in Fig. 7, **6u** led to a significant accumulation of A375 cells at G1 phase from 52.65 to 55.72% (1 μM), 60.75% (2.5 μM) and 66.86% (5 μM), accordingly,

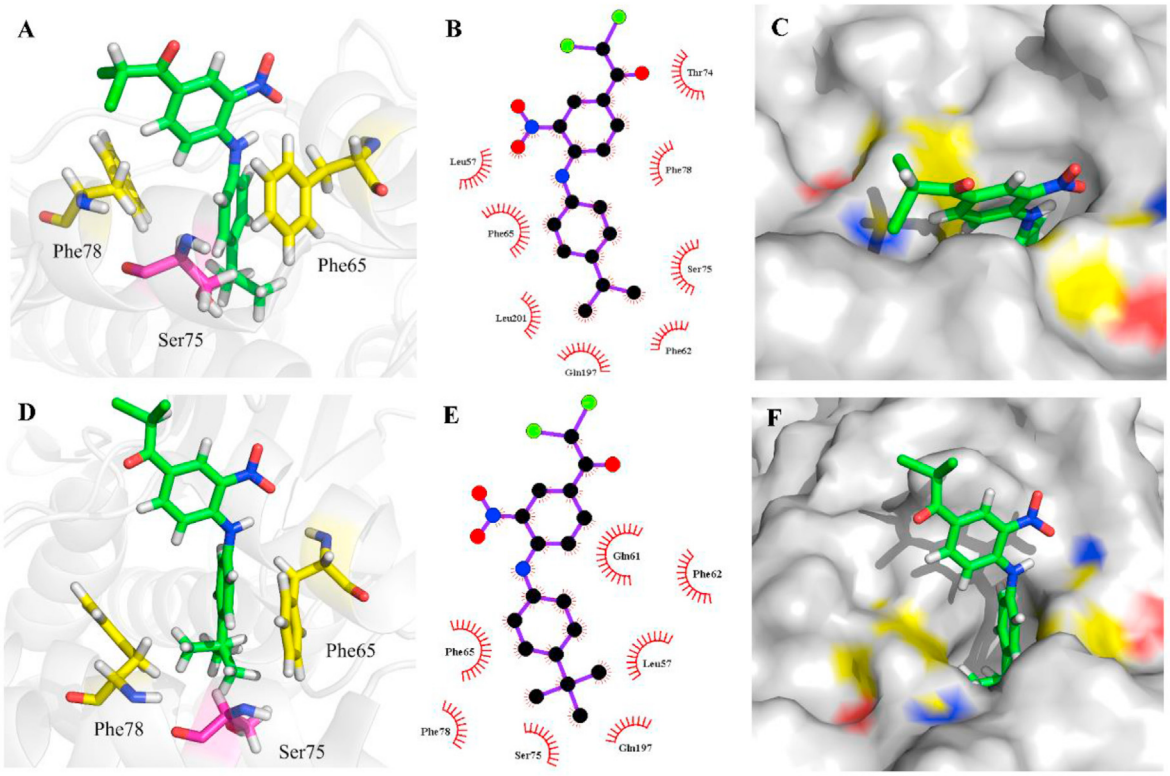

Fig. 2. Binding model of **6m** and **6s** with PDK1 (PDK code: 2Q8G). (A/D) 3D diagram of the proposed **6m**/**6s**-PDK complex; (B/E) The 2D diagram of the hydrophobic contacts between **6m**/**6s** and PDK. The plots were generated by LigPlot^{+}, the spoked arcs represent residues making non-bonded contacts with the ligand; (C/F) Stereoscopic view of **6m**/**6s** in the binding pocket of PDK. The graphics of 3D views were drawn by PyMOL, and the amino acids involved in hydrophobic interaction were shown as stick, while the Ser75 was highlighted as red.

while 58.34% for **DAP-64** at 5 μM. However, the G1 phase accumulation induced by **6u** and **DAP-64** may result from the compounds' off-target effect. At the same time, it reduced the cells at S phase from 34.63 to 27.43%, and G2 phase from 9.64% to 5.71%, respectively. The cell cycle arrest at G1 phase induced by **6u** was on concentration-dependent, which might be one of the possible mechanisms for its cytotoxicity.

2.5. Compound *6u* inhibited A375 cell migration

Cell migration was widely observed in the process of cancer cell proliferation, we therefore studied the effect of **6u** on A375 cell migration. As shown in Fig. 8A and B, the wound healing and Transwell assays indicated that A375 cell migration was significantly reduced after treating with **6u** as compared with the control group, suggesting that **6u** strongly inhibits cancer cell migration.

2.6. Compound *6u* depolarized mitochondria membrane potential (*Δψm*)

Cancer cells exhibit hyperpolarized Δψm as compared with normal cells, in which a positive voltage gradient builds across the inner mitochondrial membrane to the outside. Depolarization of the Δψm represents an effective strategy to inhibit cancer cell growth. When A375 cell was treated with **DAP-64**, or **6u** for 4 h, much reduced stain by tetramethyl rhodamine methyl ester (TMRM) was observed, suggesting mitochondrial depolarization by **6u** in the cells (Fig. 9, left). To further validate the result, we used a cationic dye, 5,5′,6,6′-tetrachloro-1,1′,3,3′-tetraethylbenzimidazolylcarbocyanine iodide (JC-1), which accumulated in mitochondria of high potential and displayed as red color due to the formation of the red fluorescent J-aggregates. Mitochondrial depolarization is indicated by an increase of the green fluorescence intensity (J-monomer) when the concentrations of **6u** is raising, as shown in Fig. 9 (right). All these suggested that **6u** depolarized the mitochondrial hyperpolarization and thus revived oxidative metabolism in cancer cell.

2.7. Compound *6u* suppressed the phosphorylation of PDK and affected the glycolysis pathway in A375 cancer cell

To verify the PDK inhibition leading to the reduction of the PDC phosphorylation level, A375 cells were treated with **6u** (1, 2.5, and 5 μM) or **DAP-64** (5 μM) for 24 h, then PDC phosphorylation was analyzed by western blotting experiment. As shown in Fig. 10A, **6u** reduced PDC phosphorylation (p(Ser^{293})E1α) level at 5 or 2.5 μM, as **DAP-64** did at 5 μM. Inhibition of PDK activates PDC, leading to a switch of pyruvate metabolism from lactate production to oxidative phosphorylation. Thus, the lactate formation and oxygen consumption (OCR) will change in cells. So next, A375 cells were treated with **DAP-64** (5 μM), or **6u** (1, 2.5, and 5 μM) for 4 h, and the changes in the intracellular lactate formation and OCR were monitored. As shown in Fig. 10B, **6u** dose independently reduced the lactate formation in A375 cells, and increased OCR in a concentration dependent manner (Fig. 10C). In addition, inhibition of PDKs would lead to an increase of mitochondria activity, therefore, reactive oxygen species (ROS) production should increase. We therefore measured the ROS production in A375 cell after treating with **6u** (1, 2.5, and 5 μM) for 4 h. As shown in Fig. 10D, more ROS was generated with higher concentrations of **6u**, indicating enhanced cellular respiration activity.

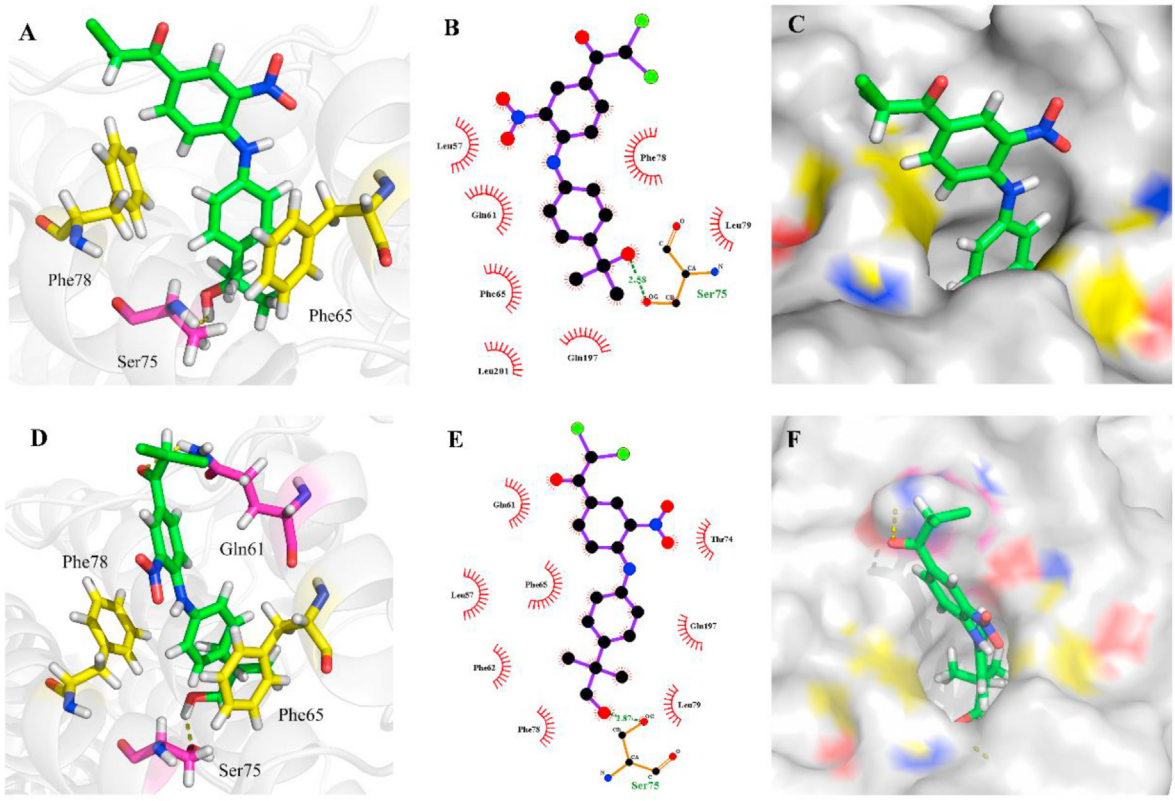

Fig. 3. Proposed binding model of **6t** and **6u** with PDK1 (PDK code: 2Q8G). (A/D) 3D diagram of the proposed **6t**/**6u**-PDK complex; (B/E) The 2D diagram of hydrogen bond interaction and hydrophobic contacts between **6t**/**6u** and PDK; (C/F) Stereoscopic view of **6t**/**6u** in the binding pocket of PDK.

*2.8. Compound **6u** suppressed tumor growth in A375 xenograft model*

Since **6u** exhibited the most potent *in vitro* anticancer activities, we next established an A375 xenograft model and performed an *in vivo* efficacy study for **6u**. Visible tumors were developed at the inoculation sites 7 days after A375 cells were inoculated subcutaneously into the animal. Tumor bearing mice were then grouped randomly (n = 4) and intramuscular injected with vehicle (5% DMSO + 95% HP-β-CD (20%)), or compound **6u** (5 mg/kg) once per three day for a continuous 21 days, respectively. As shown in the tumor growth curve in Fig. 11A, treatment of **6u** at a dose of 5 mg/kg suppressed the tumor growth, but did not affect significantly the body weight (Fig. 11C), suggesting the compound is well tolerated at the dose. At 21 days, the tumors were harvested and weighted, the vehicle group is higher than the drug administrated group (Fig. 11B).

3. Conclusions

In this paper, a series of novel PDK inhibitors with improved potencies based on the **DAP** or **DAP-64** structure has been developed. Combining their preliminarily antiproliferative activity against MCF-7 and A549 cells, and their ability to inhibit enzymatic activities, we identified a promising PDK inhibitor **6u**, which displayed good antiproliferative activities against various cancer cell lines. The PDKs enzymatic assay revealed that **6u** inhibited the enzyme with an EC_{50} value of 0.09 μM, which is a potent activity as compared to previous reported inhibitor. We also found that **6u** induced A375 cell apoptosis and arrested the cell cycle in G1 phase, and inhibited the cell migration. In addition, **6u** altered glucose metabolic profile in A375 cells by decreasing lactate formation and increasing ROS production and OCR consumption. All these data demonstrated that **6u** could be a promising lead for the development of potent PDKs inhibitors.

4. Experimental section

4.1. Chemistry

All chemicals were purchased from commercial source and used without further purification unless otherwise stated. The reactions were monitored by thin-layer chromatography and carried out on commercial Merck Kieselgel 60 F_{254} plates, which could be visualized under UV light at 254 nm. Column chromatography was performed on silica gel. ^{1}H NMR spectra were obtained on an Agilent 400 MR spectrometer, while ^{13}C NMR spectra were obtained with proton decoupling on an Agilent 400 MR DD2 (100 MHz) or 600 MR DD2 spectrometer and were reported in ppm with residual solvent for internal standard (δ 77.16 ($CDCl_3$)). The chemical shifts were reported in parts per million (ppm), the coupling constants (J) were expressed in hertz (Hz) and signals were described as singlet (s), doublet (d), triplet (t), as well as multiplet (m). The NMR data was analyzed by MestReNova software. High-resolution mass spectra were obtained on a Bruker SolariX 7.0 T spectrometer. Melting points were recorded on a WRS-2A digital melting point apparatus. All other chemicals and solvents were commercially available, and were used as received.

*4.1.1. General procedures for the synthesis of compounds **2a-d**, and **2f***

To a round-bottom flask, 2 mmol of 1-(4-bromo-3-nitrophenyl) ethanone (**1**), 3 mmol of boronic acids, 6 mmol of K_2CO_3 and 0.06 mmol of $Pd(PPh_3)_4$ were added. Then the flask was flushed

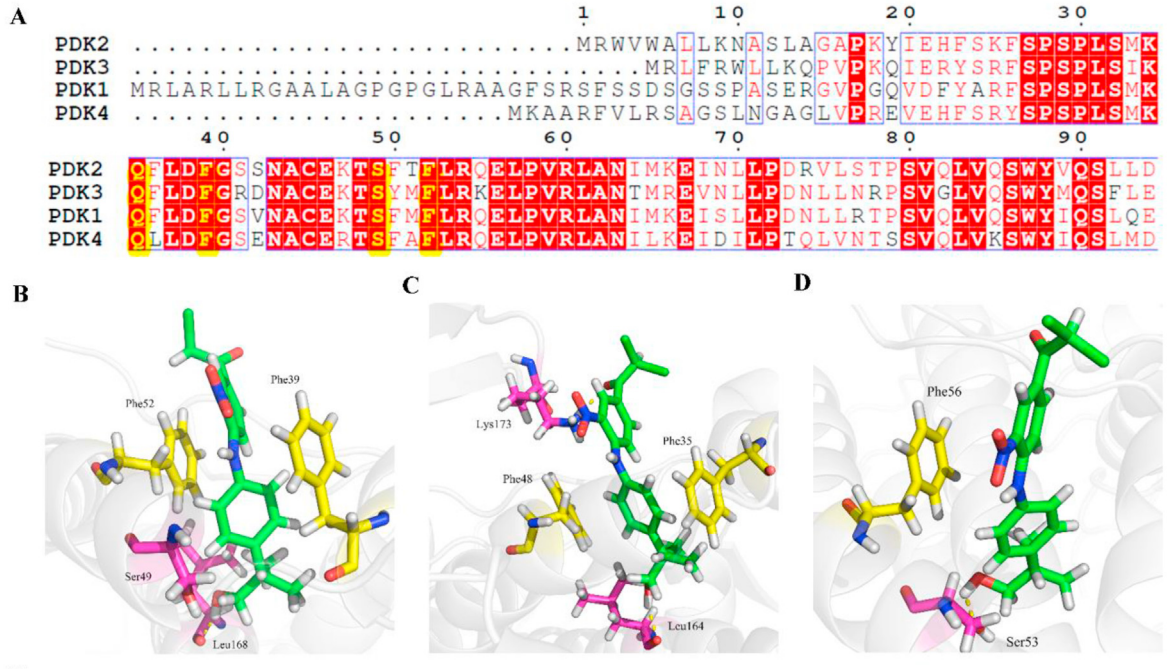

E

Isoforms	PDK1	PDK2	PDK3	PDK4
K_d (μM) [a]	0.21	ND [b]	7.8	9.2

Fig. 4. Compound **6u** bound to PDK isoforms. (A) Sequence alignment of the hydrophobic lipoamide-binding pocket of PDK1-4; (B–D) The proposed binding model of **6u** with PDK2 (PDB code: 6LIL), PDK3 (PDB code: 1Y8O), and PDK4 (PDB code: 3D2R); (4) The K_d values derived from ITC titration. [a] Compound **6u** (100 μM) was titrated into PDK1-4 (10 μM) solution. [b] not detected.

with nitrogen *via* a rubber septum, water (6 mL) and dioxane (18 L) were added. The resulting suspension was stirred, degassed and heated for 6 h at 95 °C. It was then cooled to room temperature, diluted with water, and extracted with ethyl acetate (2 x 30 mL). The combined organic layers were dried over Na_2SO_4, filtered and concentrated. The crude residue was purified by silica gel chromatography to afford the desired compounds.

1-(2-Nitrobiphenyl-4-yl)ethanone (**2a**) was obtained as a white solid after flash chromatography. M.p. 85–86 °C. ^{1}H NMR (400 MHz, $CDCl_3$): δ (ppm) 8.39 (m, 1H), 8.19–8.16 (m, 1H), 7.57 (d, J = 8 Hz, 1H), 7.45–7.44 (m, 3H), 7.32–7.34 (m, 2H), 2.68 (s, 3H); ^{13}C NMR (101 MHz, $CDCl_3$): δ (ppm) 195.51, 149.56, 140.48, 136.87, 136.42, 132.59, 131.50, 129.06, 129.00, 127.83, 124.07, 26.80.

1-(4′-Methyl-2-nitrobiphenyl-4-yl)ethanone (**2b**) was obtained as a yellow solid after flash chromatography. M.p. 82–83 °C. ^{1}H NMR (400 MHz, $CDCl_3$): δ (ppm) 8.36 (s, 1H), 8.16 (d, J = 8 Hz, 1H), 7.56 (d, J = 8 Hz, 1H), 7.27–7.21 (m, 4H), 2.67 (s, 3H), 2.41 (s, 3H); ^{13}C NMR (101 MHz, $CDCl_3$): δ (ppm) 195.56, 149.59, 140.47, 139.22, 136.60, 133.40, 132.52, 131.44, 129.77, 127.72, 124.07, 26.80, 21.42.

1-(4′-Fluoro-2-nitrobiphenyl-4-yl)ethanone (**2c**) was obtained as a white solid after flash chromatography. M.p. 95–96 °C. ^{1}H NMR (400 MHz, $CDCl_3$): δ (ppm) 8.40 (s, 1H), 8.18 (d, J = 8 Hz, 1H), 7.55 (d, J = 8 Hz, 1H), 7.33–7.30 (m, 2H), 7.17–7.13 (m, 2H), 2.69 (s, 3H); ^{13}C NMR (101 MHz, $CDCl_3$): δ (ppm) 195.41, 163.27 (d, J_F = 251 Hz), 149.51, 139.43, 137.06, 132.59, 132.44 (d, J_F = 3.3 Hz), 131.57, 129.77 (d, J_F = 8.4 Hz), 124.16, 116.11 (d, J_F = 22 Hz), 26.81.

1-(2-Nitro-4'-(trifluoromethoxy)biphenyl-4-yl)ethanone (**2d**) was obtained as a white solid after flash chromatography. M.p. 99–101 °C. ^{1}H NMR (400 MHz, $CDCl_3$): δ (ppm) 8.43 (s, 1H), 8.20 (d, J = 8 Hz, 1H), 7.56 (d, J = 8 Hz, 1H), 7.38–7.36 (m, 2H), 7.31–7.27 (m, 2H), 2.69 (s, 3H); ^{13}C NMR (101 MHz, $CDCl_3$): δ (ppm) 195.35, 149.81, 149.38, 139.12, 137.33, 135.09, 132.59, 131.71, 129.52, 124.24, 121.30, 26.80.

1-(3-Nitro-4-(thiophen-3-yl)phenyl)ethanone (**2f**) was obtained as a yellow solid after flash chromatography. M.p. 105–106 °C. ^{1}H NMR (400 MHz, $CDCl_3$): δ (ppm) 8.32 (s, 1H), 8.14 (d, J = 8 Hz, 1H), 7.63 (d, J = 8 Hz, 1H), 7.42 (m, 2H), 7.09–7.11 (m, 1H), 2.67 (s, 3H); ^{13}C NMR (101 MHz, $CDCl_3$): δ (ppm) 195.42, 149.29, 136.68, 136.00, 134.74, 132.16, 131.39, 127.12, 126.94, 124.71, 123.90, 26.78.

4.1.2. General procedure for the synthesis of compound **2e**

To a round-bottom flask, 2 mmol of 1-(4-bromo-3-nitrophenyl) ethanone (**1**), 3 mmol of cyclopropylboronic acid, 0.4 mmol of tricyclohexyl phosphine, 10 mmol of K_3PO_4 and 0.02 mmol of $Pd(OAc)_2$ were added. The flask was flushed with nitrogen *via* a rubber septum, water (1 mL) and dioxane were added, the resulting suspension was stirred, degassed and heated for 4 h at 100 °C. It was then cooled to room temperature, diluted with water, and extracted with ethyl acetate (2 x 30 mL). The combined organic layers were dried over Na_2SO_4, filtered and concentrated. The crude residue was purified by silica gel chromatography to afford the pure compound **2e**. ^{1}H NMR (400 MHz, $CDCl_3$): δ (ppm) 8.35 (s, 1H), 8.05 (d, J = 8 Hz, 1H), 7.19 (d, J = 8 Hz, 1H), 2.63 (s, 3H), 2.47–2.43 (m, 1H), 1.19–1.17 (m, 2H), 0.84–0.83 (m, 2H); ^{13}C NMR (101 MHz, $CDCl_3$): δ (ppm) 195.55, 151.13, 143.52, 135.27, 131.78, 127.58, 124.18, 26.67, 12.64, 9.67.

4.1.3. General procedure for the synthesis of compound **3a-f**

To a round-bottom flask, 6 mmol of copper (II) chloride dihydrate, 6 mmol of lithium chloride, and 1 mmol of the corresponding ketones (**2a-f**) were added. Then DMF (5 mL) was added and heated

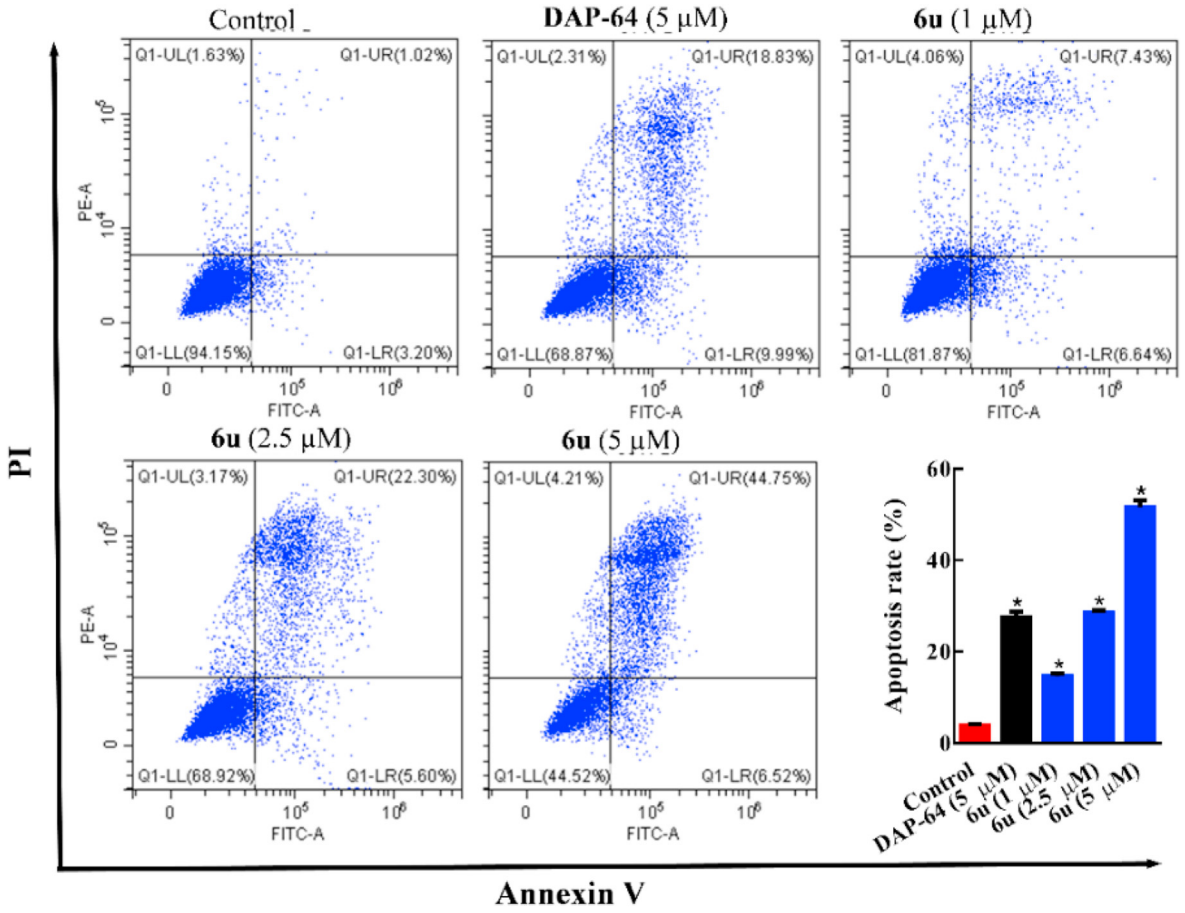

Fig. 5. Compound **6u** induced A375 cells apoptosis in a dose response manner. A375 cells were treated with **6u** at 1, 2.5, and 5 μM, or **DAP-64** at 5 μM for 36 h, then stained with FITC Annexin V/PI dyes. Cells in the upper right quadrant are PI positive/Annexin V positive, indicate late apoptotic, or necrotic cells, while cells in lower right quadrant indicate early apoptotic cells. *$P < 0.05$, versus control group.

to 90 °C for stirring 9 h. The mixture was then cooled to room temperature, diluted with water and extracted with ether (3 x 30 mL). The combined organic layers were wash with water (3 x 20 mL). The organic extract was dried over Na_2SO_4, filtered and concentrated. The crude residue was purified by silica gel chromatography to afford the pure compounds (**3a-f**).

2,2-Dichloro-1-(2-nitrobiphenyl-4-yl)ethanone (**3a**) was obtained as a yellow solid after flash chromatography. M.p. 69–70 °C; ^{1}H NMR (400 MHz, $CDCl_3$): δ (ppm) 8.56 (s, 1H), 8.35 (d, J = 8 Hz, 1H), 7.63 (d, J = 8 Hz, 1H), 7.47–7.46 (m, 3H), 7.36–7.33 (m, 2H), 6.62 (s, 1H); ^{13}C NMR (101 MHz, $CDCl_3$): δ (ppm) 184.00, 149.51, 141.80, 135.95, 133.07, 132.76, 130.86, 129.39, 129.11, 127.78, 125.67, 67.84. HRMS (ESI): calcd. for $C_{14}H_9Cl_2NNaO_3$ $[M+Na]^+$: 331.9852, found: 331.9847.

2,2-Dichloro-1-(4′-methyl-2-nitrobiphenyl-4-yl)ethanone (**3b**) was obtained as a yellow solid after flash chromatography. M.p. 84–85 °C; ^{1}H NMR (400 MHz, $CDCl_3$): δ (ppm) 8.53 (s, 1H), 8.33 (d, J = 8 Hz, 1H), 7.62 (d, J = 8 Hz, 1H), 7.29–7.25 (m, 4H), 6.60 (s, 1H), 2.41 (s, 3H); ^{13}C NMR (101 MHz, $CDCl_3$): δ (ppm) 184.03, 149.60, 141.83, 139.67, 132.98, 132.68, 130.61, 129.90, 127.71, 125.67, 67.87, 21.45. HRMS (ESI): calcd. for $C_{15}H_{11}Cl_2NNaO_3$ $[M+Na]^+$: 346.0008, found: 346.0003.

2,2-Dichloro-1-(4′-fluoro-2-nitrobiphenyl-4-yl)ethanone (**3c**) was obtained as a yellow liquid after flash chromatography. ^{1}H NMR (400 MHz, $CDCl_3$): δ (ppm) 8.56 (s, 1H), 8.35 (d, J = 8 Hz, 1H), 7.60 (d, J = 8 Hz, 1H), 7.34–7.30 (m, 2H), 7.17–7.13 (m, 2H), 6.61 (s, 1H); ^{13}C NMR (101 MHz, $CDCl_3$): δ (ppm) 183.94, 161.39 (d, J_F = 251 Hz), 149.43, 140.71, 133.14, 132.73, 131.97 (d, J_F = 3.4 Hz), 131.05, 129.76 (d, J_F = 9.1 Hz), 125.74, 116.29 (d, J_F = 22.1 Hz), 67.83. HRMS (ESI): calcd. for $C_{14}H_7Cl_2FNO_3$ $[M-H]^-$: 325.9793, found: 325.9785.

2,2-Dichloro-1-(2-nitro-4'-(trifluoromethoxy)biphenyl-4-yl) ethanone (**3d)** was obtained as a yellow liquid after flash chromatography. ^{1}H NMR (400 MHz, $CDCl_3$): δ (ppm) 8.62 (s, 1H), 8.38 (d, J = 8 Hz, 1H), 7.61 (d, J = 8 Hz, 1H), 7.40–7.38 (m, 2H), 7.33–7.31 (m, 2H), 6.59 (s, 1H); ^{13}C NMR (101 MHz, $CDCl_3$): δ (ppm) 183.93, 150.05, 149.38, 140.44, 134.61, 133.33, 132.74, 131.35, 129.52, 125.91, 121.42, 67.88. HRMS (ESI): calcd. for $C_{15}H_7Cl_2F_3NO_4$ $[M-H]^-$: 392.9710, found: 391.9701.

2,2-Dichloro-1-(4-cyclopropyl-3-nitrophenyl)ethanone (**3e**) was obtained as a yellow solid after flash chromatography. M.p. 54–55 °C; ^{1}H NMR (400 MHz, $CDCl_3$): δ (ppm) 8.52 (s, 1H), 8.21 (d, J = 8 Hz, 1H), 7.22 (d, J = 8 Hz, 1H), 6.58 (s, 1H), 2.48 (m, 1H), 1.24–1.22 (m, 2H), 0.89–0.87 (m, 2H); ^{13}C NMR (101 MHz, $CDCl_3$): δ (ppm) 183.96, 151.15, 145.40, 133.35, 129.16, 127.58, 125.72, 67.83, 12.82, 10.30. HRMS (ESI): calcd. for $C_{11}H_8Cl_2NO_3$ $[M-H]^-$: 271.9887, found: 271.9880.

2,2-Dichloro-1-(3-nitro-4-(thiophen-3-yl)phenyl)ethanone (**3f**) was obtained as a yellow solid after flash chromatography. M.p. 92–93 °C; ^{1}H NMR (400 MHz, $CDCl_3$): δ (ppm) 8.50 (s, 1H), 8.32 (d, J = 8 Hz, 1H), 7.68 (d, J = 8 Hz, 1H), 7.47–7.44 (m, 2H), 7.13–7.12 (m, 1H), 6.58 (s, 1H); ^{13}C NMR (101 MHz, $CDCl_3$): δ (ppm) 183.92, 149.26, 136.07, 135.61, 132.96, 132.28, 130.64, 127.24, 127.01, 125.55, 125.27, 67.86. HRMS (ESI): calcd. for $C_{12}H_6Cl_2NO_3S$ $[M-H]^-$: 313.9451, found: 313.9443.

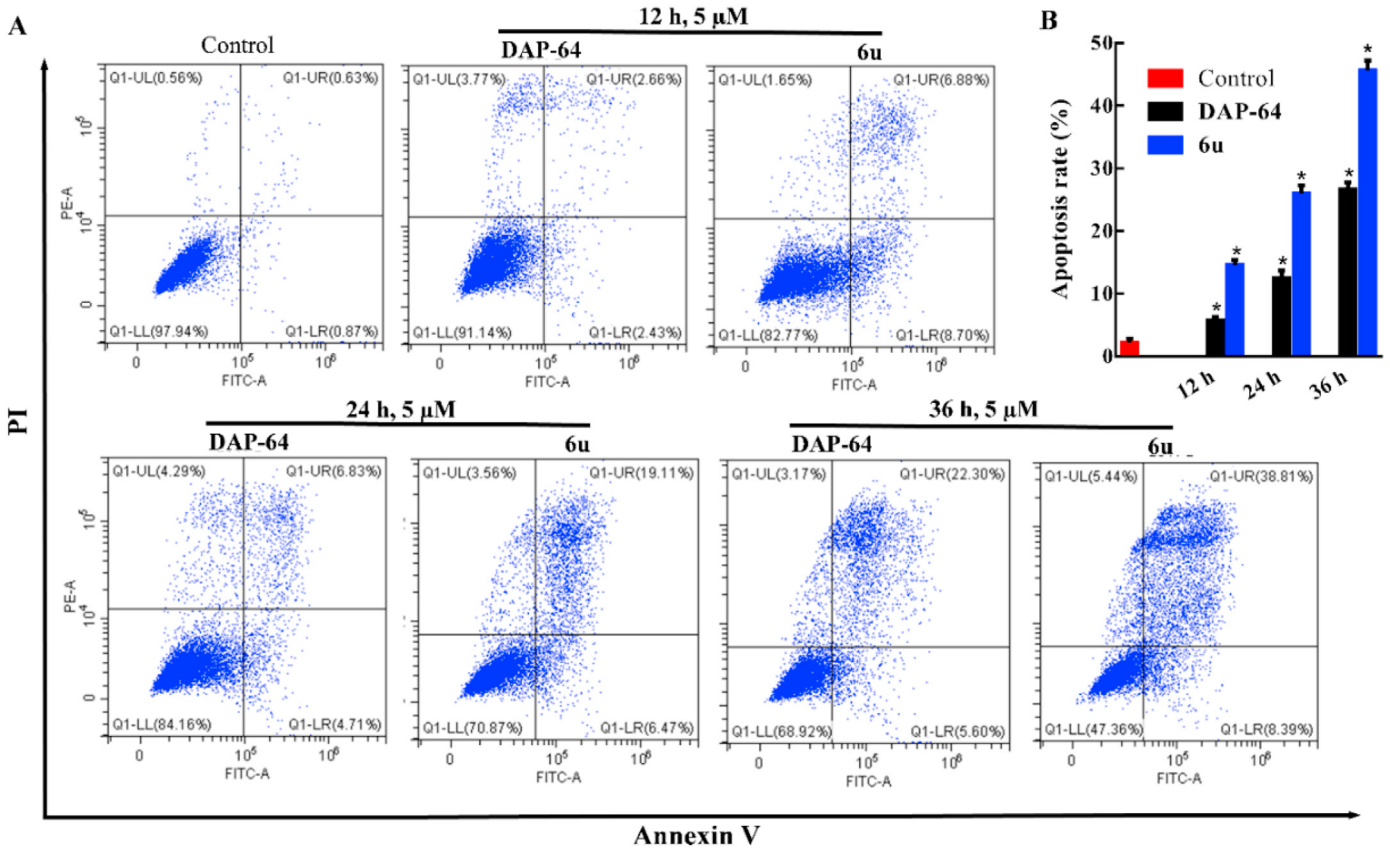

Fig. 6. Compound **6u** induced A375 cell apoptosis in a time-dependent manner. A375 cells were treated with **6u** at 5 μM, or **DAP-64** at 5 μM for 12, 24, 36 h, respectively, then stained with FITC Annexin V/PI dyes. *$P < 0.05$, versus control group.

*4.1.4. General procedure for the synthesis of compound **5***

A mixture of 8.0 mmol of NH_4Cl, 10.0 mmol of 1-(4-fluoro-3-nitrophenyl) ethanone, and 20 mL of acetonitrile was stirred for 5 min, then 15 mmol 1,3-dichloro-5,5-dimethylhydantoin was added by five times within 1 h, and the mixture was stirred at 35 °C for 18 h. Afterward, solvent was distilled under reduced pressure, 100 mL of ethyl acetate was added to the residue. The ethyl acetate layer was washed with water (2 x 30 mL), the organic layers was dried over Na_2SO_4, filtered and concentrated. The crude residue was purified by silica gel chromatography to afford a colorless oil **5**. ^{1}H NMR (400 MHz, $CDCl_3$): δ (ppm) 8.85–8.83 (m, 1H), 8.47–8.43 (m, 1H), 7.51–7.47 (m, 1H), 6.57 (s, 1H); ^{13}C NMR (101 MHz, $CDCl_3$): δ (ppm) 183.11, 160.10, 157.37, 137.07 (d, $J_F = 10.0$ Hz), 128.52, 127.80 (d, $J_F = 4.0$ Hz), 119.56 (d, $J_F = 22.0$ Hz), 67.72 (d, $J_F = 4.0$ Hz).

*4.1.5. General procedure for the synthesis of compound **6a-s***

To a round-bottom flask, 0.2 mmol of 2,2-dichloro-1-(4-fluoro-3-nitrophenyl)ethan-1-one (**5**), 0.25 mmol of various primary amines or secondary amines, 0.25 mmol K_2CO_3, and DMF (0.5 mL) were added. The reaction mixture was stirred for 3 h at room temperature. The mixture was diluted with ethyl acetate (150 mL). The organic layers were wash with water (3 x 20 mL), the organic extract was dried over Na_2SO_4, filtered and concentrated. The crude residue was purified by silica gel chromatography to afford the pure compounds **6a-s**.

2,2-Dichloro-1-(4-(cyclopropylamino)-3-nitrophenyl)ethanone (**6a**) was obtained as a yellow solid after flash chromatography. M.p. 104–105 °C; ^{1}H NMR (400 MHz, $CDCl_3$): δ (ppm) 8.98–8.97 (m, 1H), 8.55 (s, 1H), 8.20 (d, $J = 8$ Hz, 1H), 7.41 (d, $J = 8$ Hz, 1H), 6.59 (s, 1H), 2.70 (m, 1H), 1.04–1.02 (m, 2H), 0.76–0.75 (m, 2H); ^{13}C NMR (101 MHz, $CDCl_3$): δ (ppm) 183.51, 149.64, 136.31, 131.44, 130.18, 119.03, 115.83, 67.83, 24.96, 8.17. HRMS (ESI): calcd. for $C_{11}H_9Cl_2N_2O_3$ $[M-H]^-$: 286.9996, found: 271.9989.

2,2-Dichloro-1-(3-nitro-4-(pyrrolidin-1-yl)phenyl)ethanone (**6b**) was obtained as a yellow solid after flash chromatography. M.p. 103–104 °C; ^{1}H NMR (400 MHz, $CDCl_3$): δ (ppm) 8.48 (s, 1H), 8.05 (d, $J = 9.2$ Hz, 1H), 6.93 (d, $J = 9.2$ Hz, 1H), 6.58 (s, 1H), 3.34 (m, 4H), 2.05 (m, 4H); ^{13}C NMR (101 MHz, $CDCl_3$): δ (ppm) 183.17, 145.64, 136.15, 133.64, 129.88, 117.77, 115.94, 67.88, 50.96, 25.69. HRMS (ESI): calcd. for $C_{12}H_{12}Cl_2N_2NaO_3$ $[M+Na]^+$: 325.0117, found: 325.0113.

2,2-Dichloro-1-(4-morpholino-3-nitrophenyl)ethanone (**6c**) was obtained as a yellow solid after flash chromatography. M.p. 111–112 °C; ^{1}H NMR (400 MHz, $CDCl_3$): δ (ppm) 8.56 (d, $J = 2.4$ Hz, 1H), 8.20–8.17 (m, 1H), 7.12 (d, $J = 8.8$ Hz, 1H), 6.55 (s, 1H), 3.86 (t, $J = 4.8$ Hz, 4H), 3.27 (t, $J = 4.8$ Hz, 4H); ^{13}C NMR (101 MHz, $CDCl_3$): δ (ppm) 183.32, 149.21, 139.54, 134.81, 129.63, 121.91, 119.20, 67.85, 66.35, 50.87. HRMS (ESI): calcd. for $C_{12}H_{11}Cl_2N_2O_4$ $[M-H]^-$: 317.0101, found: 317.0094.

2,2-Dichloro-1-(3-nitro-4-(piperidin-1-yl)phenyl)ethanone (**6d**) was obtained as a yellow solid after flash chromatography. M.p. 64–65 °C; ^{1}H NMR (400 MHz, $CDCl_3$): δ (ppm) 8.52 (s, 1H), 8.10 (d, $J = 9.2$ Hz, 1H), 7.10 (d, $J = 9.2$ Hz, 1H), 6.57 (s, 1H), 3.25–3.24 (m, 4H), 1.72 (m, 6H); ^{13}C NMR (101 MHz, $CDCl_3$): δ (ppm) 183.26, 149.74, 138.51, 134.38, 130.02, 120.11, 119.28, 67.86, 51.81, 25.63, 23.79. HRMS (ESI): calcd. for $C_{13}H_{13}Cl_2N_2O_3$ $[M-H]^-$: 315.0309, found: 315.0301.

2,2-Dichloro-1-(3-nitro-4-(piperazin-1-yl)phenyl)ethanone (**6e**) was obtained as a yellow liquid after flash chromatography. ^{1}H NMR (400 MHz, $CDCl_3$): δ (ppm) 8.56 (s, 1H), 8.18–8.15 (m, 1H), 7.11

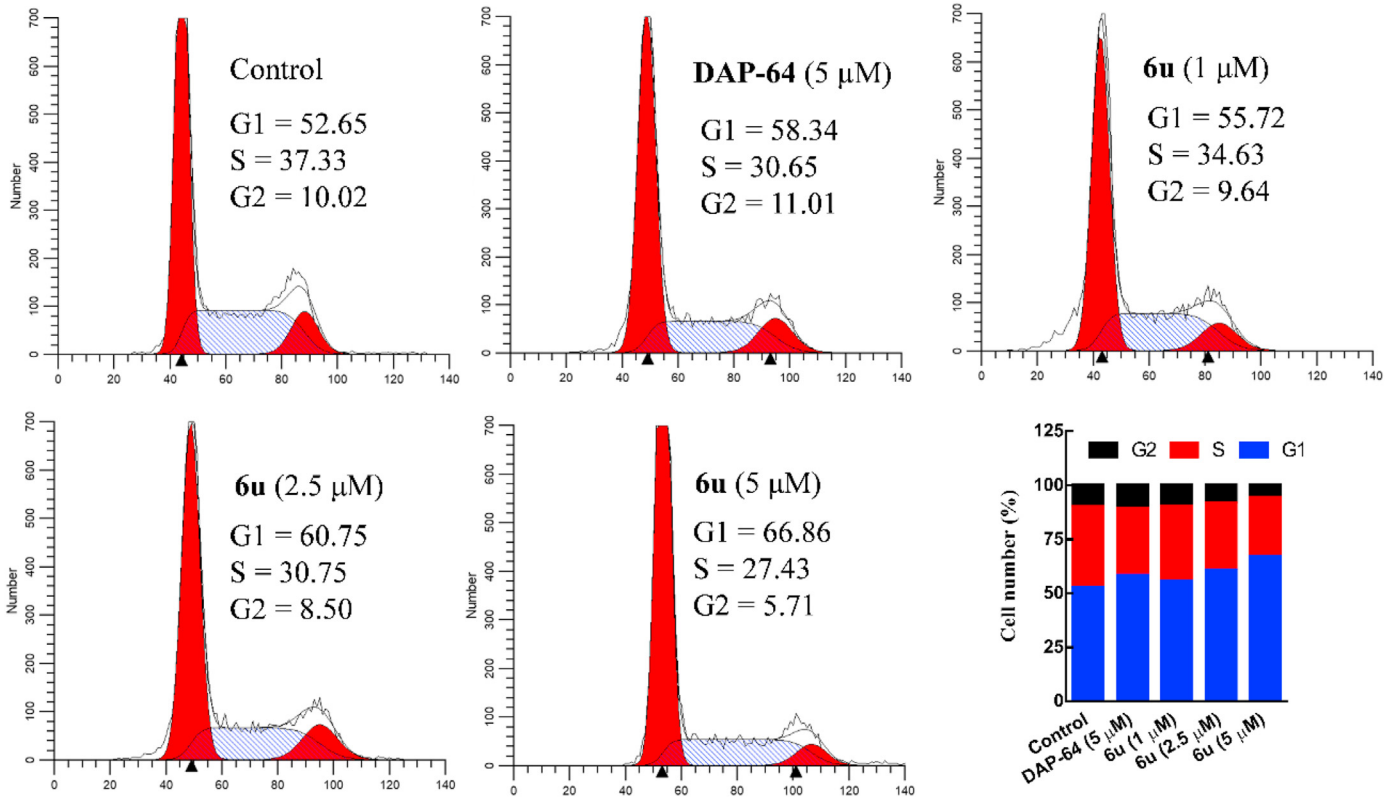

Fig. 7. Compound **6u** induced cell cycle arrest in A375 cells. Cells were treated with **6u** at 1, 2.5 and 5 μM or **DAP-64** at 5 μM for 24 h, then were harvested, washed with PBS, and fixed in 70% cold ethanol. After incubation overnight, the cell pellets were collected by centrifugation, re-suspended in 50 mg/mL of RNase A in PBS. Then PI dye (50 mg/mL) was added, and the mixture was incubated at 37 °C for 15 min. Cell cycle analysis was performed *via* flow cytometer. Bar graph represents the values of cells in G1, S, and G2 phases.

(d, J = 8.8 Hz, 1H), 6.53 (s, 1H), 3.29–3.28 (m, 4H), 3.09–3.08 (m, 4H); ^{13}C NMR (101 MHz, $CDCl_3$): δ (ppm) 183.35, 149.48, 139.44, 134.75, 129.77, 121.57, 119.48, 67.90, 51.49, 45.48. HRMS (ESI): calcd. for $C_{12}H_{14}Cl_2N_3O_3$ $[M+H]^+$: 318.0407, found: 318.0401.

1-(4-(1-Imidazol-1-yl)-3-nitrophenyl)-2,2-dichloroethanone (**6f**) was obtained as a yellow liquid after flash chromatography. ^{1}H NMR (400 MHz, $CDCl_3$): δ (ppm) 8.73 (s, 1H), 8.50 (d, J = 8 Hz, 1H), 7.71 (s, 1H), 7.66 (d, J = 8 Hz, 1H), 7.27 (s, 1H), 7.12 (s, 1H), 6.58 (s, 1H); ^{13}C NMR (101 MHz, $CDCl_3$): δ (ppm) 183.24, 144.97, 136.92, 134.82, 131.58, 131.42, 128.65, 127.27, 119.80, 67.83. HRMS (ESI): calcd. for $C_{11}H_6Cl_2N_2O_3$ $[M-H]^-$: 297.9792, found: 297.9785.

2,2-Dichloro-1-(3-nitro-4-(1H-1,2,4-triazol-1-yl)phenyl)ethanone (**6g**) was obtained as a yellow liquid after flash chromatography. ^{1}H NMR (400 MHz, $CDCl_3$): δ (ppm) 8.73–8.72 (m, 1H), 8.54–8.51 (m, 2H), 8.18 (s, 1H), 7.82 (d, J = 8.4 Hz, 1H), 6.56 (s, 1H); ^{13}C NMR (101 MHz, $CDCl_3$): δ (ppm) 183.17, 153.83, 143.83, 134.71, 133.89, 132.06, 127.31, 127.12, 67.80. HRMS (ESI): calcd. for $C_{10}H_5Cl_2N_4O_3$ $[M-H]^-$: 298.9744, found: 298.9737.

2,2-Dichloro-1-(3-nitro-4-(2-nitro-1H-imidazol-1-yl)phenyl) ethanone (**6h**) was obtained as a yellow solid after flash chromatography. M.p. 163–164 °C; ^{1}H NMR (400 MHz, $CDCl_3$): δ (ppm) 9.05 (s, 1H), 8.61 (d, J = 8 Hz, 1H), 7.69 (d, J = 8 Hz, 1H), 7.41 (s, 1H), 7.20 (s, 1H), 6.62 (s, 1H); ^{13}C NMR (101 MHz, $CDCl_3$): δ (ppm) 183.04, 141.90, 135.73, 135.03, 133.46, 130.25, 130.04, 127.82, 125.67, 67.80. HRMS (ESI): calcd. for $C_{11}H_5Cl_2N_4O_5$ $[M-H]^-$: 342.9643, found: 342.9634.

2,2-Dichloro-1-(3-nitro-4-(phenylamino)phenyl)ethanone (**6i**) was obtained as a yellow solid after flash chromatography. M.p. 120–121 °C; ^{1}H NMR (400 MHz, $CDCl_3$): δ (ppm) 9.98 (s, 1H), 9.03 (m, 1H), 8.08–8.06 (m, 1H), 7.52–7.48 (m, 2H), 7.38–7.31 (m, 3H), 7.21–7.18 (m, 1H), 6.58 (s, 1H); ^{13}C NMR (101 MHz, $CDCl_3$): δ (ppm) 183.26, 147.09, 137.02, 136.11, 131.97, 130.33, 130.23, 127.54, 125.55, 120.01, 116.15, 67.83. HRMS (ESI): calcd. for $C_{14}H_9Cl_2N_2O_3$ $[M-H]^-$: 322.9996, found: 322.9988.

2,2-Dichloro-1-(4-(4-methoxyphenylamino)-3-nitrophenyl) ethanone (**6j**) was obtained as a yellow solid after flash chromatography. M.p. 125–126 °C; ^{1}H NMR (400 MHz, $CDCl_3$): δ (ppm) 9.87 (s, 1H), 9.02 (m, 1H), 8.03 (d, J = 8 Hz, 1H), 7.23–7.21 (m, 2H), 7.05–6.99 (m, 3H), 6.58 (s, 1H); ^{13}C NMR (101 MHz, $CDCl_3$): δ (ppm) 183.29, 159.03, 148.02, 136.03, 131.57, 130.35, 129.50, 127.54, 119.56, 116.14, 115.42, 67.82, 55.73. HRMS (ESI): calcd. for $C_{15}H_{11}Cl_2N_2O_4$ $[M-H]^-$: 353.0101, found: 353.0092.

2,2-Dichloro-1-(3-nitro-4-(p-tolylamino)phenyl)ethanone (**6k**) was obtained as a yellow solid after flash chromatography. M.p. 140–141 °C; ^{1}H NMR (400 MHz, $CDCl_3$): δ (ppm) 9.93 (s, 1H), 9.02 (s, 1H), 8.04 (d, J = 9.2 Hz, 1H), 7.30–7.26 (m, 2H), 7.20–7.12 (m, 3H), 6.58 (s, 1H), 2.42 (s, 3H); ^{13}C NMR (101 MHz, $CDCl_3$): δ (ppm) 183.30, 147.51, 137.70, 136.04, 134.27, 131.73, 130.81, 130.37, 125.63, 119.72, 116.21, 67.82, 21.24. HRMS (ESI): calcd. for $C_{15}H_{11}Cl_2N_2O_3$ $[M-H]^-$: 337.0152, found: 337.0146.

2,2-Dichloro-1-(4-(4-ethoxyphenylamino)-3-nitrophenyl)ethanone (**6l**) was obtained as a yellow solid after flash chromatography. M.p. 92–93 °C; ^{1}H NMR (400 MHz, $CDCl_3$): δ (ppm) 9.87 (s, 1H), 9.02 (s, 1H), 8.03 (d, J = 9.2 Hz, 1H), 7.20 (d, J = 8.4 Hz, 2H), 7.04 (d, J = 9.2 Hz, 1H), 6.99 (d, J = 8.4 Hz, 2H), 6.58 (s, 1H), 4.08 (q, J = 6.8 Hz, 2H), 1.46 (t, J = 6.8 Hz, 3H); ^{13}C NMR (101 MHz, $CDCl_3$): δ (ppm) 183.29, 158.42, 148.05, 136.02, 131.52, 130.36, 129.29, 127.51, 119.50, 116.17, 115.90, 67.82, 63.99, 14.91. HRMS (ESI): calcd. for $C_{16}H_{13}Cl_2N_2O_4$ $[M-H]^-$: 367.0258, found: 367.0249.

2,2-Dichloro-1-(4-(4-isopropylphenylamino)-3-nitrophenyl) ethanone (**6m**) was obtained as a yellow solid after flash chromatography. M.p. 133–134 °C; ^{1}H NMR (400 MHz, $CDCl_3$): δ (ppm) 9.95

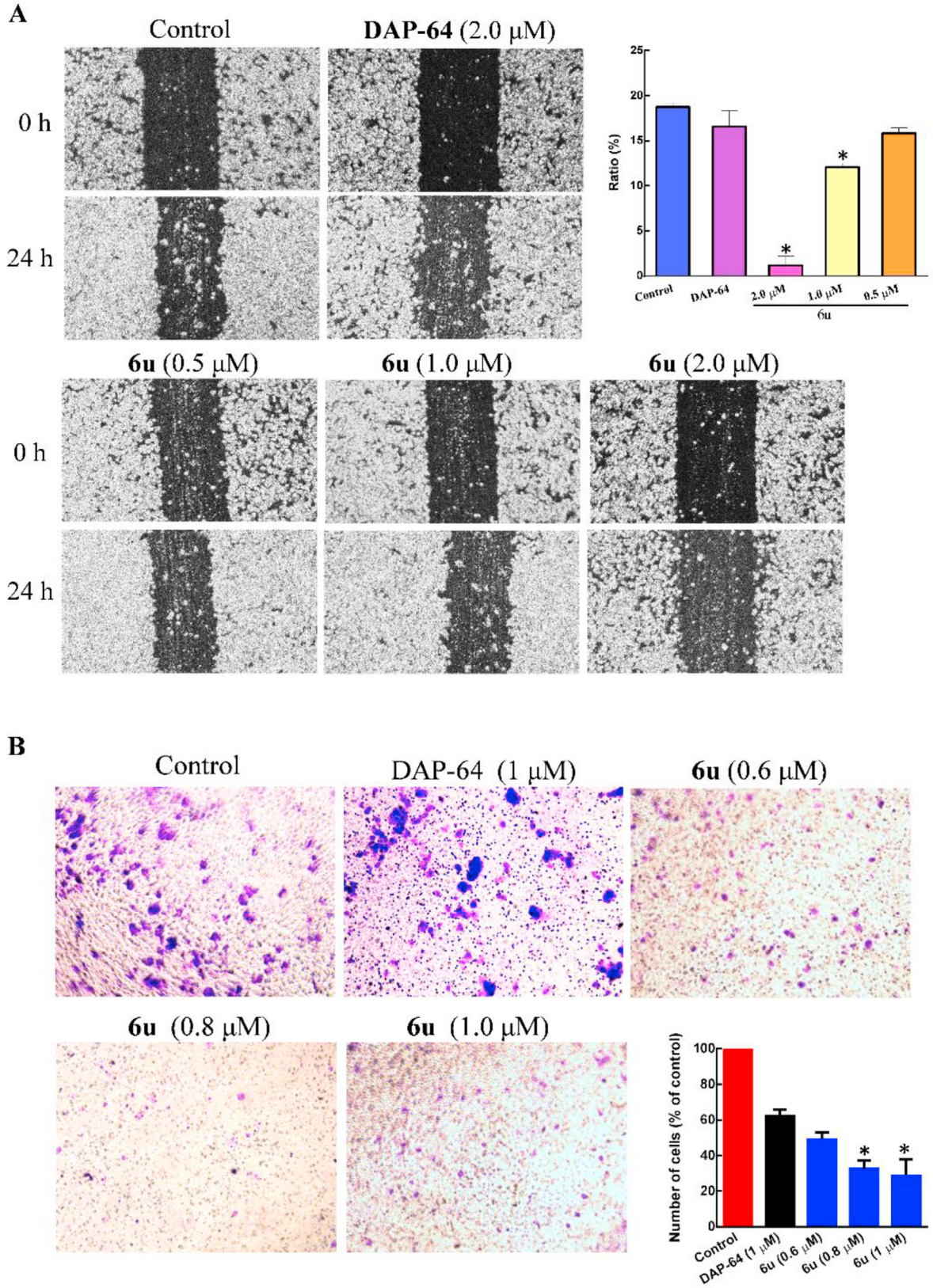

Fig. 8. Compound **6u** inhibited A375 cell invasion and migration. A375 cells were treated with **6u** (0.5, 1.0, and 2.0 μM) or **DAP-64** (2.0 μM) for 24 h in wound healing assay, while **6u** (0.6, 0.8, and 1 μM) or **DAP-64** (1 μM) was used in Transwell assays. (A) The upper photo showed the closure of A375 cells after being scratched (× 100) for 24 h, the ration (%) was calculated by (start scratched area-after scratched area)/start scratched area; (B) The A375 cells were seeded onto chambers, and incubated with **6u** or **DAP-64** for 24 h. Cells migrated through the chambers were stained with crystal violet, and representative images were captured. The graph indicate the changes of scratch area or number of cells vs the control group. *$P < 0.05$, versus control group.

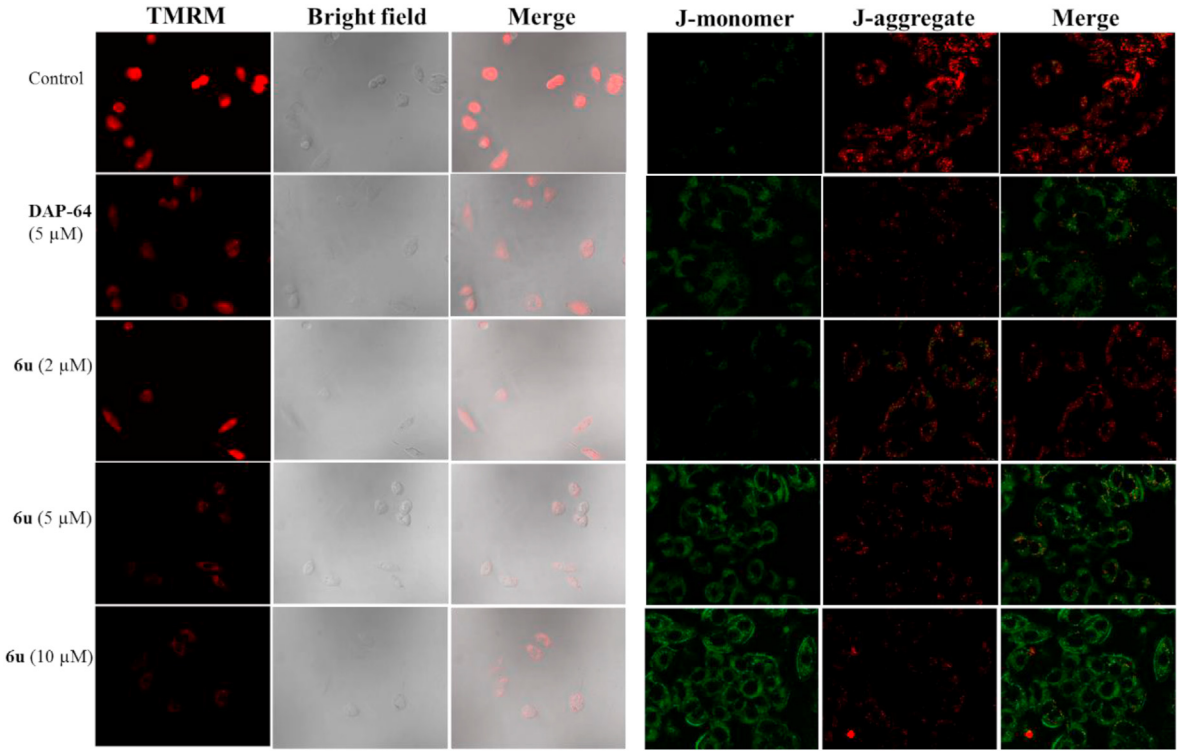

Fig. 9. Depolarization of Δψm in A375 cell by **6u**. Cell was treated with PBS, or **DAP-64** (5 μM), or **6u** (2, 5, and 10 μM) at 37 °C for 4 h and stained by TMRM (left) or JC-1 (right), then analyzed with confocal microscopy. Scale bar for TMRM image is 10 μM, while 25 μM for JC-1 image.

(s, 1H), 9.02 (s, 1H), 8.07–8.04 (m, 1H), 7.35–7.33 (m, 2H), 7.22 (m, 2H), 7.17 (d, J = 9.2 Hz, 1H), 6.58 (s, 1H), 3.01–2.94 (m, 1H), 1.29 (d, J = 7.2 Hz, 6H); ^{13}C NMR (101 MHz, $CDCl_3$): δ (ppm) 183.29, 148.61, 147.45, 136.03, 134.50, 131.73, 130.37, 128.19, 125.61, 119.72, 116.27, 67.83, 33.94, 24.08. HRMS (ESI): calcd. for $C_{17}H_{15}Cl_2N_2O_3$ [M-H]$^-$: 365.0465, found: 365.0456.

2,2-Dichloro-1-(4-(3,4-dimethoxyphenylamino)-3-nitrophenyl)ethanone (**6n**) was obtained as a black solid after flash chromatography. M.p. 143–144 °C; ^{1}H NMR (400 MHz, $CDCl_3$): δ (ppm) 9.74 (s, 1H), 9.04 (m, 1H), 8.09 (d, J = 9.2 Hz, 1H), 7.02 (s, 1H), 6.89–6.86 (m, 2H), 6.59 (s, 1H), 3.94 (s, 3H), 3.88 (s, 3H); ^{13}C NMR (101 MHz, $CDCl_3$): δ (ppm) 183.29, 149.29, 148.87, 147.15, 136.20, 132.01, 130.17, 126.43, 122.99, 120.22, 116.19, 112.98, 110.92, 67.80, 56.53, 29.80. HRMS (ESI): calcd. for $C_{16}H_{13}Cl_2N_2O_5$ [M-H]$^-$: 383.0207, found: 383.0198.

2,2-Dichloro-1-(4-(4-(dimethylamino)phenylamino)-3-nitrophenyl)ethanone (**6o**) was obtained as a black solid after flash chromatography. M.p. 165–166 °C; ^{1}H NMR (400 MHz, $CDCl_3$): δ (ppm) 9.87 (s, 1H), 9.01 (m, 1H), 8.00 (d, J = 9.2 Hz, 1H), 7.13 (d, J = 8.8 Hz, 2H), 7.05 (d, J = 9.2 Hz, 1H), 6.77 (d, J = 8.8 Hz, 2H), 6.58 (s, 1H), 3.02 (s, 6H); ^{13}C NMR (101 MHz, $CDCl_3$): δ (ppm) 183.34, 149.94, 148.51, 135.84, 131.26, 130.45, 127.14, 125.21, 119.10, 116.43, 113.17, 67.81, 40.67. HRMS (ESI): calcd. for $C_{16}H_{14}Cl_2N_3O_3$ [M-H]$^-$: 366.0418, found: 366.0410.

2,2-Dichloro-1-(4-((4-fluorophenyl)amino)-3-nitrophenyl) ethan-1-one (**6p**) was obtained as a pure solid after flash chromatography. M.p. 145–146 °C. ^{1}H NMR (400 MHz, $CDCl_3$): δ (ppm) 9.88 (s, 1H), 9.03 (m, 1H), 8.08 (d, J = 8 Hz, 1H), 7.32–7.27 (m, 2H), 7.22–7.18 (m, 2H), 7.07 (d, J = 8 Hz, 1H), 6.58 (s, 1H); ^{13}C NMR (101 MHz, $CDCl_3$): δ (ppm) 183.26, 161.63 (d, J_F = 249 Hz), 147.40, 136.25, 132.94 (d, J_F = 3 Hz), 131.91, 130.31, 127.92 (d, J_F = 8.6 Hz), 120.06, 117.24 (d, J_F = 23 Hz), 115.90, 67.82. HRMS (ESI): calcd. for $C_{14}H_8Cl_2FN_2O_3$ [M-H]$^-$: 340.9902, found: 340.9888.

2,2-Dichloro-1-(4-(4-isopropylphenoxy)-3-nitrophenyl)ethan-1-one (**6q**) was obtained as a white solid after flash chromatography. M.p. 71–72 °C. ^{1}H NMR (400 MHz, $CDCl_3$): δ (ppm) 8.70 (s, 1H), 8.21 (d, J = 4 Hz, 1H), 7.31 (d, J = 8 Hz, 2H), 7.06 (d, J = 8 Hz, 2H), 7.01 (d, J = 8 Hz, 1H), 6.52 (s, 1H), 2.99–2.92 (m, 1H), 1.28 (s, 3H), 1.27 (s, 3H); ^{13}C NMR (101 MHz, $CDCl_3$): δ (ppm) 183.24, 156.34, 151.36, 147.17, 139.85, 135.30, 128.40, 128.01, 124.43, 120.46, 117.98, 67.69, 33.64, 24.02. HRMS (ESI): calcd. for $C_{17}H_{14}Cl_2NO_4^-$ ([M-H]$^-$) 366.0305, found 366.0293.

2,2-Dichloro-1-(4-((4-isopropylphenyl)thio)-3-nitrophenyl) ethan-1-one (**6r**) was obtained as a pale yellow oil after flash chromatography. ^{1}H NMR (400 MHz, $CDCl_3$): δ (ppm) 8.97 (s, 1H), 8.05 (d, J = 8 Hz, 1H), 7.51 (d, J = 8 Hz, 2H), 7.40 (d, J = 8 Hz, 2H), 7.00 (d, J = 8 Hz, 1H), 6.54 (s, 1H), 3.05–2.98 (m, 1H), 1.33 (s, 3H), 1.32 (s, 3H); ^{13}C NMR (101 MHz, $CDCl_3$): δ (ppm) 183.76, 152.29, 148.48, 144.27, 136.06, 133.34, 128.88, 128.53, 127.57, 127.34, 126.06, 67.82, 34.21, 23.93. HRMS (ESI): calcd. for $C_{17}H_{14}Cl_2NO_3S^-$ ([M-H]$^-$) 382.0077, found 382.0062.

1-(4-((4-(Tert-butyl)phenyl)amino)-3-nitrophenyl)-2,2-dichloroethan-1-one (**6s**) was obtained as reddish brown solid after flash chromatography. M.p. 106–107 °C. ^{1}H NMR (400 MHz, $CDCl_3$): δ (ppm) 9.95 (s, 1H), 9.04 (d, J = 4 Hz, 1H), 8.06 (d, J = 8 Hz, 1H), 7.50 (d, J = 12 Hz, 2H), 7.25 (d, J = 8 Hz, 2H), 7.22 (s, 1H), 6.57 (s, 1H), 1.36 (s, 9H); ^{13}C NMR (101 MHz, $CDCl_3$): δ (ppm) 183.33, 150.90, 147.43, 136.07, 134.22, 131.76, 130.42, 127.14, 125.24, 119.73, 116.31, 67.84, 34.89, 31.46. HRMS (ESI): calcd. for $C_{18}H_{17}Cl_2N_2O_3^-$ ([M-H]$^-$) 379.0622, found 379.0606.

4.1.6. General procedure for the synthesis of compound **6t**

To a round-bottom flask, 30 mmol of 1-(4-aminophenyl)ethan-1-one (**7**) was dissolved in THF (180 mL), then CH_3MgBr (150 mmol, 40 mL) was added. The mixture was stirred in −10 °C for 3 h. After completion of the reaction, the mixture was quenched by NH_4Cl

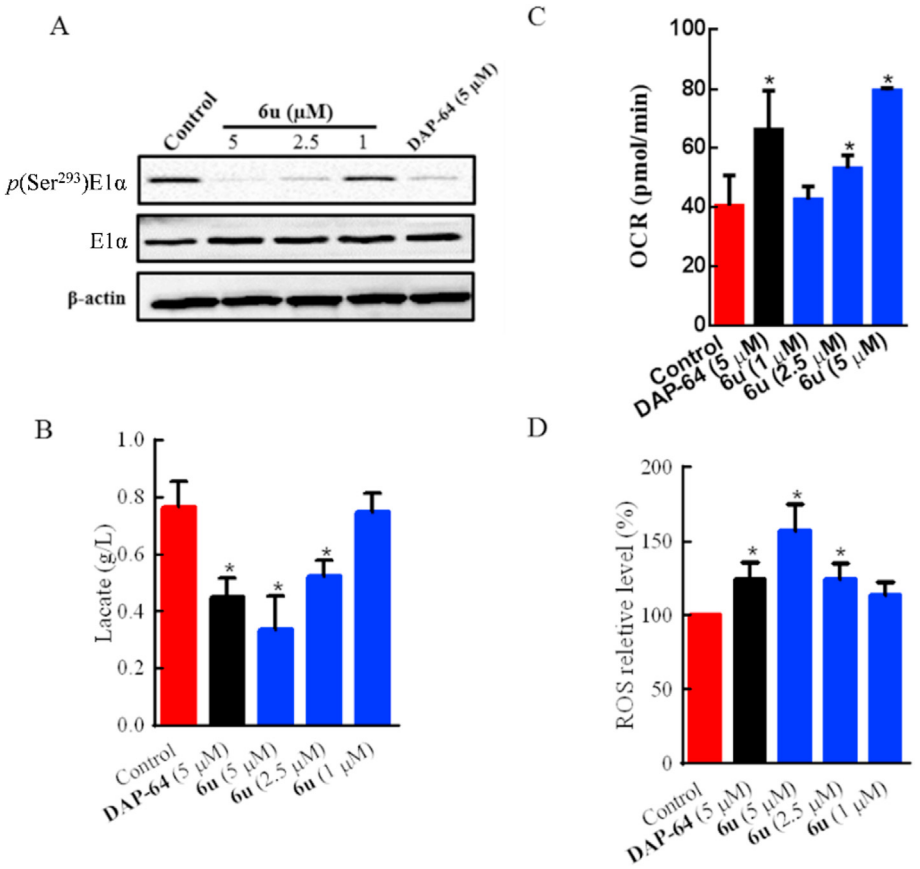

Fig. 10. The effect of compound **6u** on the glycolysis pathway in A375 cells. (A) Compounds **6u** exhibited dose response manner to inhibit p(Ser^{293})E1α in A375 cells; (B) Compounds **6u** affected the lactate formation in A375 cell; (C) Compound **6u** increased OCR in A375 cell; (D) Compound **6u** dose-independently increased ROS production in A375 cell. *$P < 0.05$, versus control group.

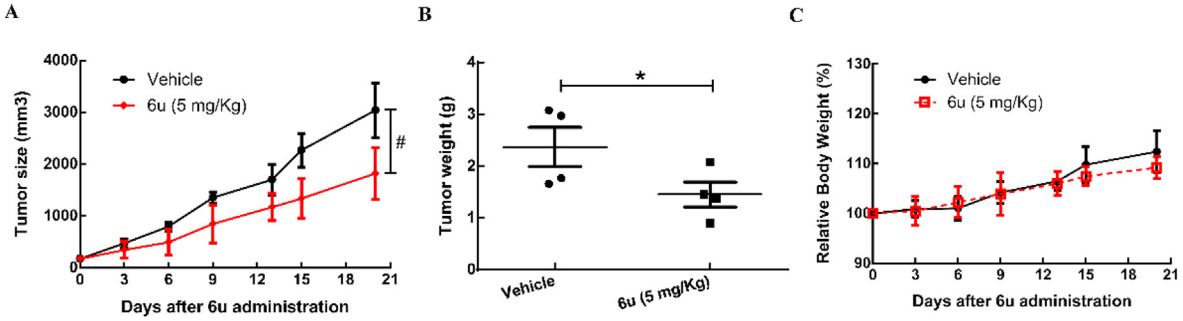

Fig. 11. Compound **6u** reduced tumor growth in A375 xenograft model. A: Average tumor volume changes during 21 days of drug exposure; B: After 21 days, the tumors were harvested and weighted; (C) Body weigh changes of mice during 21 days of drug exposure. $^{\#}P < 0.05$ and * $P < 0.05$ between Vehicle and **6u** (5 mg/kg).

solution, and the THF was removed, then was diluted with ethyl acetate (50 mL). The organic layers were wash with water (3 x 50 mL), the organic extract was dried over Na_2SO_4, filtered and concentrated. The crude residue (**8**) was then dissolved in DMF (10 mL), and added compound **5** and potassium carbonate. The mixture was stirred at room temperature for 12 h. After completion of the reaction, the mixture was diluted with ethyl acetate (50 mL) and water (50 mL). The organic layers were wash with water (3 x 50 mL), the organic extract was dried over Na_2SO_4, filtered and concentrated. Compound **6t** was purified by silica gel chromatography to afford the reddish brown solid. M.p. 96–97 °C. ^{1}H NMR (400 MHz, $CDCl_3$): δ (ppm) 9.96 (s, 1H), 9.03 (s, 1H), 8.06 (d, J = 12 Hz, 1H), 7.61 (d, J = 8 Hz, 2H), 7.27 (d, J = 8 Hz, 2H), 7.20 (d, J = 12 Hz, 1H), 6.56 (s, 1H), 1.78 (s, 1H), 1.63 (s, 6H); ^{13}C NMR (101 MHz, $CDCl_3$): δ (ppm) 183.30, 148.64, 147.17, 136.09, 135.41, 131.88, 130.35, 126.38, 125.25, 119.91, 116.22, 72.51, 67.81, 31.99. HRMS (ESI): calcd. for $C_{17}H_{15}Cl_2N_2O_4^-$ ([M-H]$^-$) 381.0414, found 381.0399.

4.1.7. General procedure for the synthesis of compound ***11***

To a round-bottom flask, 50 mmol of 2-(4-nitrophenyl)acetic acid (**9**) and MeOH (60 mL) mixture together, then concentrated sulfuric acid (5 mL) was added. The mixture was refluxed for 6 h. After completion of the reaction, the mixture was quenched by water, then MeOH was removed, and diluted with ethyl acetate (50 mL). The organic layers were wash with water (3 x 50 mL), the

organic extract was dried over Na_2SO_4, filtered and concentrated. The crude residue (**10**) was then dissolved in DMF (10 mL), then CH_3I and sodium hydroxide was added. The mixture was stirred at 0 °C for 24 h. After completion of the reaction, the mixture was diluted with ethyl acetate (50 mL) and water (50 mL). The organic layers were wash with water (3 x 50 mL), the organic extract was dried over Na_2SO_4, filtered and concentrated. Compound **11** was purified by silica gel chromatography to afford a white solid. M.p. 40–41 °C. ^{1}H NMR (400 MHz, $CDCl_3$): δ (ppm) 8.15 (d, J = 8.0 Hz, 2H), 7.48 (d, J = 8.0 Hz, 2H), 3.65 (s, 3H), 1.60 (s, 6H); ^{13}C NMR (101 MHz, $CDCl_3$): δ (ppm) 176.07, 152.00, 146.75, 126.90, 123.65, 52.60, 47.01, 26.46.

4.1.8. General procedure for the synthesis of compound **12**

To a round-bottom flask, compound **11** (5.0 g, 22.4 mmol) and THF (40 mL) were added, then DIBAL-H (67.0 mL, 67.2 mmol) was added dropwise. The mixture was stirred at 0 °C for 24 h. After completion of the reaction, the mixture was quenched by NH_4Cl solution, then diluted with ethyl acetate (50 mL). The organic layers were collected and washed with water (3 x 50 mL). The organic extract was dried over Na_2SO_4, filtered and concentrated. Compound **12** was purified by silica gel chromatography to afford a pale yellow solid. M.p. 60–61 °C. ^{1}H NMR (400 MHz, $CDCl_3$): δ (ppm) 8.16 (d, J = 8.0 Hz, 2H), 7.55 (d, J = 8.0 Hz, 2H), 3.67 (s, 3H), 1.61 (s, 1H), 1.37 (s, 6H); ^{13}C NMR (101 MHz, $CDCl_3$): δ (ppm) 154.92, 146.23, 127.39, 123.44, 72.42, 40.78, 25.32.

4.1.9. General procedure for the synthesis of compound **13**

A mixture of compound **12** (2.0 g, 10.2 mmol) and 10% Pd/C (200 mg, 0.2 mmol) in EtOH (20 mL) was evacuated and back-filled with H_2. The mixture was stirred at room temperature for 12 h. After completion of the reaction, the mixture was filtered and the solvent was evaporated *in vacuo*. The crude product was purified by flash chromatography to provide a colorless oil **13**. ^{1}H NMR (400 MHz, $CDCl_3$): δ (ppm) 7.16 (d, J = 8.0 Hz, 2H), 6.65 (d, J = 12.0 Hz, 2H), 3.51 (s, 2H), 2.99 (br, 3H), 1.28 (s, 6H); ^{13}C NMR (101 MHz, $CDCl_3$): δ (ppm) 144.40, 136.32, 127.16, 115.24, 73.11, 39.30, 25.43.

4.1.10. General procedure for the synthesis of compound **6u**

A mixture of compound **13** (236 mg, 1.43 mmol), compound **5** (300 mg, 1.2 mmol) and potassium carbonate in DMF (10 mL) was stirred at room temperature for 12 h. After completion of the reaction, the mixture was diluted with ethyl acetate (20 mL). The organic layers were collected and washed with water (3 x 20 mL). The organic extract was dried over Na_2SO_4, filtered and concentrated. Compound **6u** was purified by silica gel chromatography to afford a reddish brown solid. M.p. 90–91 °C. ^{1}H NMR (400 MHz, $CDCl_3$): δ (ppm) 9.95 (s, 1H), 9.02 (s, 1H), 8.06 (d, J = 12 Hz, 1H), 7.50 (d, J = 8 Hz, 2H), 7.27 (d, J = 8 Hz, 2H), 7.21 (d, J = 8 Hz, 1H), 6.57 (s, 1H), 3.67 (s, 2H), 1.53 (s, 1H), 1.37 (s, 6H); ^{13}C NMR (101 MHz, $CDCl_3$): δ (ppm) 183.13, 146.98, 146.09, 135.92, 134.79, 131.70, 130.21, 127.96, 125.17, 119.73, 116.09, 72.77, 67.66, 40.04, 25.37. HRMS (ESI): calcd. for $C_{18}H_{17}Cl_2N_2O_4^-$ ([M-H]$^-$) 395.0571, found 395.0553.

4.2. Biological evaluation

4.2.1. Cell culture

A549, MCF-7, SHSY-5Y, HCT-116, A375, PC-3 and L02 cell lines were purchased from Shanghai Cell Bank of Chinese Academy of Sciences (Shanghai, China), which were cultured in DMEM medium and supplemented with 10% FBS, 1% penicillin and streptomycin at 37 °C in a 5% CO_2 humidified atmosphere. Cells grown at exponential stage were used for all the biological experiments.

4.2.2. Cell viability assay

Cell viability after treated with the prepared compounds and **DAP**, **DAP-64** were tested by using the MTT assay. A suspension of cells (3000–6000/well for cancer cell lines, and 7000/well for L02) were seeded in 96-well plates and cultured overnight. Then two concentrations of all synthesized compounds (100, and 10 μM, PBS buffer containing 1% DMSO) were added into the 96-well plates, in which cells were incubated for 72 h. Then, 10 μL of MTT (0.5 mg/mL) solution was added to each well of the plates. After 4 h incubation, the supernatant was removed and 100 μL of DMSO was added. The absorbance of each well was measured at 570 nm in a microplate reader. After identified the potential compounds, the full dose concentration of desired compounds (**6m**, **6s**, **6t**, and **6u**) was measured, resultant $OD_{570\ nm}$ values were expressed as IC_{50} values, which were the mean values derived from three independent experiments.

4.2.3. Lactate measurement

Suspension of A375 cells (2.5×10^5/well) were seeded in 24-well plates and cultured overnight. Then **DAP-64** (5 μM) and **6u** (1, 2.5, and 5 μM) were added to the corresponding wells, the plates were incubated at 37 °C for 4 h. Then the medium was transferred into EP tubes, which were centrifuged for 4 min (12000 rpm/min). At last, 1 mL of medium was collected, which was used to test the lactate production on a Nova Bioprofile Flex analyzer.

4.2.4. OCR measurement

The OCR was measured as previous report [17]. A375 cells (5 x 10^4/well) were cultured in XF24-well cell culture microplates (Seahorse Bioscience) in 100 μL growth medium and incubated for 1 h at 37 °C in 5% CO_2 atmosphere. After the cells were attached, an additional 100 μL growth medium was added and the cells were incubated for another 24 h, which was then treated with **DAP-64** (5 μM), **6u** (1, 2.5, and 5 μM) for 4 h. The culture medium was then removed and the cells were rinsed two times with 100 μL of pre-warmed XF^e base medium. Finally 170 μL of XF^e cell Mito stress test assay medium was added to each well and the plate was placed at 37 °C without CO_2 for 1 h prior to measurement.

4.2.5. ITC analysis

Proteins was prepared to 10 μM in the buffer solution (20 mM KH_2PO_4/K_2HPO_4, 100 mM KCl, and 1 mM MgCl2). Compound **6u** was dissolved in pure DMSO and diluted to 100 μM by using the buffer solution. Then 250 μL of proteins solution were transferred to reaction cell and the compound solution was transferred to the titration syringe. Titrations were conducted with the injection of 2.5 μL titrant in every increment into the reaction cell, which was maintained at 25 °C.

4.2.6. ROS measurement

A375 cells were seeded at a density of 4×10^4 cells/mL on a dark, clear bottom 96-well plates and were allowed to grow overnight. Then culture medium was removed and a diluted DCFH-DA solution was added (100 μL/well) to incubate the cells for 45 min at 37 °C. Remove the medium and washed with 1 × PBS for three times. Then the cells were treated with **6u** (1, 2.5, and 5 μM), and **DAP-64** (5 μM) at 37 °C for 4 h. At last, the plate was measured on a microplate reader at Ex/Em = 485/535 nm.

4.2.7. PDKs inhibitory potency assay

The PDKs inhibitory potency assay was measured as previous report [24].

4.2.8. Cell cycle assay

A375 cells were seeded in 6-well plates at density of

$1-2 \times 10^5$ cells/well and treated with **6u** (1, 2.5 and 5 μM) for 24 h. Then, cells were harvested and fixed in 70% pre-cooled ethanol. Finally, cells were stained by PI/RNase A and measured by a flow cytometer (Accuri C6, BD Biosciences).

4.2.9. Cell apoptosis assay

A375 cells were seeded at a density of $1-2 \times 10^5$ cells/well on 6-well plates and allowed to grow overnight. The cells were treated with **6u** (1, 2.5 and 5 μM) or **DAP-64** (5 μM) for 24 h. Then the cells were trypsinized, repeatedly washed with cold PBS for three times, centrifuged at 1200 rpm/min for 5 min, and the supernatants were discarded. Then cells were stained by a FITC Annexin V/PI kit in the binding buffer for 15 min at room temperature. Subsequently, cells were measured by a flow cytometer (Accuri C6, BD Biosciences).

4.2.10. Western blotting

A375 cells were seeded in 6-well plates and treated with **6u** (1, 2.5, and 5 μM), and **DAP-64** (5 μM) for 24 h. Then the treated cells were incubated with cell lysate buffer for 15 min, and centrifuged with the speed of 12000 rpm/min at 4 °C for 15 min. Protein concentrations were assessed by Pierces BCA Protein Assay Kit and balanced to the same level, followed by a 8 min protein denaturation with SDS loading buffer at 100 °C. Proteins in the samples were separated by SDS-PAGE electrophoresis, transferred onto nitrocellulose filter membrane, blocked in 5% fat free milk for 2 h, breezed with desired primary antibodies overnight, followed with secondary HRP-conjugated anti-rabbit IgG for 2 h. Membranes were finally scanned in a ChemiDoc MP Imaging System (Bio-Rad) after 2 min incubation in Clarity Western ECLSubstrate (Bio-Rad).

4.2.11. JC-1 and TMRM assay for mitochondria membrane potential

A375 cells were seeded as 4 x 10^4 cells/mL and allowed to grow overnight at 37 °C. Cells were then treated with **DAP-64** (5 μM) or **6u** (1, 2.5, and 5 μM) for 4 h at 37 °C. Then a solution of 0.5 μM JC-1 or TMRM reagents in fresh medium was added and incubated at 37 °C for 15 min. Then the culture medium was removed. The cells were washed 3 times with cool PBS, the depolarized mitochondria membrane potential was recorded in a Laser scanning confocal microscope (Leica TCS SP8).

4.2.12. Animal study

The animal study was approved by the Laboratory Animal Welfare and Ethics Committee of the Third Military Medical University. Each animal was housed under standard conditions and had free access to food and water. A375 cells at 80% confluence were harvested with trypsin/EDTA, and resuspended in serum-free DMEM medium. Cells were then inoculated in the right flank of each mouse subcutaneously. Within days after inoculation, the tumor bearing mice were randomly assigned into 2 treatment groups (4 mice/group) of vehicle, 6u (5 mg/kg) and treated with compound by intramuscular injection once per three days. Tumor volume and body weight of each mouse were recorded once per three days. Then, tumor samples were harvested and weighted.

4.2.13. Molecular docking

Molecular docking was performed using a Sybyl-X 2.0 software. The crystal structure of PDKs protein was downloaded from the Protein Data Bank (PDB ID: 2Q8G). The crystal structure of PDKs was optimized with H added and charge added by AMBER7 FF99 method. The structures of small molecular database were subjected to the polar H adding and being energy optimized with a tripos force field and charged optimized with Gasteiger-Huckel method. The graphics of 3D views were drawn by PyMOL, and the amino acids involved in hydrophobic interaction were shown as stick. Plots were generated by LigPlot$^+$, the spoked arcs represent residues making non-bonded contacts with the ligand.

4.2.14. Statistical analysis

Data was reported as Mean ± SD. Statistical analysis was performed using GraphPad Prism version 6.0 for Windows. $^*P < 0.05$ was considered as statistically significant.

Declaration of competing interest

The authors declare that they have no known competing financial interests or personal relationships that could have appeared to influence the work reported in this paper.

Acknowledgements

This work was supported by the National Natural Science Foundation of China (No. 21807008), Chongqing Science and Technology Bureau (csts2019jcyj-zdxmX0021), the Science and Technology Development Fund, Macau SAR (File no. 0057/2018/A2) and University of Macau (File no. MYRG2019-00034-FHS).

Appendix A. Supplementary data

Supplementary data to this article can be found online at https://doi.org/10.1016/j.ejmech.2021.113225.

References

[1] J.L. Counihan, E.A. Grossman, D.K. Nomura, Cancer metabolism: current understanding and therapies, Chem. Rev. 118 (2018) 6893–6923.
[2] M.G. Vander Heiden, L.C. Cantley, C.B. Thompson, Understanding the Warburg effect: the metabolic requirements of cell proliferation, Science 324 (2009) 1029–1033.
[3] M.V. Liberti, J.W. Locasale, The Warburg effect: how does it benefit cancer cells? Trends Biochem. Sci. 41 (2016) 211–218.
[4] S.L. Zhang, X.H. Hu, W. Zhang, H.K. Yao, K.Y. Tam, Development of pyruvate dehydrogenase kinase inhibitors in medicinal chemistry with particular emphasis as anticancer agents, Drug Discov. Today 20 (2015) 1112–1119.
[5] S.L. Zhang, Y. He, K.Y. Tam, Targeting cancer metabolism to develop human lactate dehydrogenase (hLDH) 5 inhibitors, Drug Discov, Today Off. 23 (2018) 1407–1415.
[6] W. Zhang, S.L. Zhang, X.H. Hu, K.Y. Tam, Targeting tumor metabolism for cancer treatment: is pyruvate dehydrogenase kinases (PDKs) a viable anticancer target? Int. J. Biol. Sci. 11 (2015) 1390–1400.
[7] T. McFate, A. Mohyeldin, H. Lu, J. Thakar, J. Henriques, N.D. Halim, H. Wu, M.J. Schell, T.M. Tsang, O. Teahan, S. Zhou, J.A. Califano, N.H. Jeoung, R.A. Harris, A. Verma, Pyruvate dehydrogenase complex activity controls metabolic and malignant phenotype in cancer cells, J. Biol. Chem. 283 (2008) 22700–22708.
[8] G. Chen, L. Wang, S. Liu, C. Chuang, T.E. Roche, Activated function of the pyruvate dehydrogenase phosphatase through Ca^{2+}-facilitated binding to the inner lipoyl domain of the dihydrolipoyl acetyltransferase, J. Biol. Chem. 271 (1996) 28064–28070.
[9] C.A. Brautigam, R.M. Wynn, J.L. Chuang, D.T. Chuang, Subunit and catalytic component stoichiometries of an *in vitro* reconstituted human pyruvate dehydrogenase complex, J. Biol. Chem. 284 (2009) 13086–13098.
[10] H. Hur, Y. Xuan, Y.B. Kim, G. Lee, W. Shim, J. Yun, I.H. Ham, S.U. Han, Expression of pyruvate dehydrogenase kinase-1 in gastric cancer as a potential therapeutic target, Int. J. Oncol. 42 (2013) 44–54.
[11] M.I. Koukourakis, A. Giatromanolaki, G. Bougioukas, E. Sivridis, Lung cancer: a comparative study of metabolism related protein expression in cancer cells and tumor associated stroma, Canc. Biol. Ther. 6 (2007) 1476–1479.
[12] (a) S.M. Wigfield, S.C. Winter, A. Giatromanolaki, J. Taylor, M.L. Koukourakis, A.L. Harris, PDK-1 regulates lactate production in hypoxia and is associated with poor prognosis in head and neck squamous cancer, Br. J. Canc. 98 (2008) 1975–1984;
(b) M.I. Koukourakis, A. Giatromanolaki, E. Sivridis, K.C. Gatter, A.L. Harris, Pyruvate dehydrogenase and pyruvate dehydrogenase kinase expression in non-small cell lung cancer and tumor-associated stroma, Neoplasia 7 (2005) 1–6.
[13] T. Meng, D.D. Zhang, Z.Q. Xie, T. Yu, S.C. Wu, L. Wyder, U. Regenass, K. Hilpert, M. Huang, M.Y. Geng, J.K. Shen, Discovery and optimization of 4,5-diarylisoxazoles as potent dual inhibitors of pyruvate dehydrogenase kinase and heat shock protein 90, J. Med. Chem. 57 (2014) 9832–9843.
[14] P.A. Brough, L. Baker, S. Bedford, K. Brown, S. Chavda, V. Chell, J. D'Alessandro, N.G.M. Davies, B. Davis, L.L. Strat, A.T. Macias, D. Maddox, P.C. Mahon,

A.J. Massey, N. Matassova, S. McKenna, J.W.G. Meissner, J.D. Moore, J.B. Murray, C.J. Northfield, C. Parry, R. Parsons, S.D. Roughley, T. Shaw, H. Simmonite, S. Stokes, A. Surgenor, E. Stefaniak, A. Robertson, Y.K. Wang, P. Webb, N. Whitehead, M. Wood, Application of off-rate screening in the identification of novel pan-isoform inhibitors of pyruvate dehydrogenase kinase, J. Med. Chem. 60 (2017) 2271−2286.

[15] W.Y. Sun, Z.Q. Xie, Y.F. Liu, D. Zhao, Z.X. Wu, D.D. Zhang, H. Lv, S. Tang, N. Jin, H.L. Jiang, M.J. Tan, J. Ding, C. Luo, J. Li, M. Huang, M.Y. Geng, JX06 selectively inhibits pyruvate dehydrogenase kinase PDK1 by a covalent cysteine modification, Canc. Res. 75 (2015) 4923−4936.

[16] Y.F. Liu, Z.Q. Xie, D. Zhao, J. Zhu, F. Mao, S. Tang, H. Xu, C. Luo, M.Y. Geng, M. Huang, J. Li, Development of the first generation of disulfide-based subtype-selective and potent covalent pyruvate dehydrogenase kinase 1 (PDK1) inhibitors, J. Med. Chem. 60 (2017) 2227−2244.

[17] S.L. Zhang, X.H. Hu, W. Zhang, K.Y. Tam, Unexpected discovery of dichloroacetate derived adenosine triphosphate competitors targeting pyruvate dehydrogenase kinase to inhibit cancer proliferation, J. Med. Chem. 59 (2016) 3562−3568.

[18] S.C. Tso, M.L. Lou, C.Y. Wu, W.J. Gui, J.L. Chuang, L.K. Morlock, N.S. Williams, R.M. Wynn, X.B. Qi, D.T. Chuang, Development of dihydroxyphenyl sulfonylisoindoline derivatives as liver-targeting pyruvate dehydrogenase kinase inhibitors, J. Med. Chem. 60 (2017) 1142−1150.

[19] B. Xu, Z.M. Yu, S.C. Xiang, Y.S. Li, S.L. Zhang, Y. He, Rational design of mitochondria-targeted pyruvate dehydrogenase kinase 1 inhibitors with improved selectivity and antiproliferative activity, Eur. J. Med. Chem. 155 (2018) 275−284.

[20] I. Papandreou, T. Goliasova, N.C. Denko, Anticancer drugs that target metabolism: is dichloroacetatethe new paradigm? Int. J. Canc. 128 (2011) 1001−1008.

[21] E.D. Michelakis, G. Sutendra, P. Dromparis, L. Webster, A. Haromy, E. Niven, C. Maguire, T.L. Gammer, J.R. Mackey, D. Fulton, B. Abdulkarim, M.S. McMurtry, K.C. Petruk, Metabolic modulation of glioblastoma with dichloroacetate, Sci. Transl. Med. 2 (2010) 31ra34.

[22] P.W. Stacpoole, T.L. kurtz, Z. Han, T. Langaee, Role of dichloroacetate in the treatment of genetic mitochondrial diseases, Adv. Drug Deliv. Rev. 60 (2008) 1478−1487.

[23] J. Espinal, T. Leesnitzer, A. Hassman, M. Beggs, J. Cobb, Inhibition of pyruvate dehydrogenase kinase by halogenated acetophenones, Drug Dev. Res. 35 (1995) 130−136.

[24] S.L. Zhang, Z. Yang, X.H. Hu, H. Chakravarty, K.Y. Tam, Anticancer effects of some novel dichloroacetophenones through the inhibition of pyruvate dehydrogenase kinase, Eur. J. Pharmaceut. Sci. 123 (2018) 43−55.

[25] S.L. Zhang, Z. Yang, X.H. Hu, K.Y. Tam, Dichloroacetophenones targeting at pyruvate dehydrogenase kinase 1 with improved selectivity and antiproliferative activity: synthesis and structure activity relationships, Bioorg. Med. Chem. Lett 28 (2018) 3441−3445.

[26] S.C. Xiang, D. Huang, Q.L. He, J. Li, K.P. Tam, S.L. Zhang, Y. He, Development of dual inhibitors targeting pyruvate dehydrogenase kinases and human lactate dehydrogenase A: high-throughput virtual screening, synthesis and biological validation, Eur. J. Med. Chem. 203 (2020), 155 112579.